Modellering van geulen, platen en drempels in de Westerschelde [1]

projectnummer: RKZ–536
projectleider: Drs. H. Verbeek

Faserapport 2

One–dimensional long–term equilibria of tidal embayments and their linear stability

(met een Nederlandse samenvatting)

H.M. Schuttelaars

[1] Dit project is uitgevoerd in opdracht van het Rijksinstituut voor Kust en Zee te Middelburg

OPDRACHTGEVER:	Rijksinstituut voor Kust en Zee van het Directoraat Generaal Rijkswaterstaat Middelburg
TITEL:	Modellering van geulen, platen en drempels in de Westerschelde

SAMENVATTING:

In dit project zal een geïdealiseerd, nietlineair model worden ontwikkeld voor een estuarium met karakteristieken als die van de Westerschelde, teneinde het dynamisch gedrag van geulen en zandplaten te onderzoeken. Daarbij ligt de nadruk op het analyseren van fysische mechanismen, die aanleiding geven tot een aantal specifieke karakteristieken, nl.

- meandergedrag van geulen
- het cyclisch gedrag van kortsluitgeulen, die de verbinding vormen tussen de hoofdgeulen
- de vorming van zogeheten drempels

Het onderzoek bestaat uit een drietal fasen:

- Verkenning Westerschelde en experimenten met een 1D model.
- Vergelijking uitkomsten 1D model met beschikbare veldgegevens en numerieke modellen en numerieke modellen, alsmede lineaire stabiliteitsanalyse van het 2D model.
- Vergelijking uitkomsten 2D model met beschikbare veldgegevens en numerieke modellen, alsmede niet–lineaire experimenten met het 2D model.

In dit rapport zijn de bevindingen uit de tweede fase vastgelegd.

Inhoudsopgave

Lijst van figuren

Nederlandse samenvatting

Algemeen kader

Door sterke wisselwerking tussen de waterbeweging en bodemvormen zijn estuaria en zeegaten morfodynamisch zeer actieve gebieden, zowel in de ruimte als in de tijd. Om deze gebieden effectief te beheren is het noodzakelijk kwantitatieve voorspellingen te kunnen maken van waterstanden, stromingen, transportprocessen en bodemontwikkelingen. De huidige modellen die de beheerder tot zijn beschikking heeft zijn in staat dit dynamische gedrag te simuleren op een tijdschaal van dagen tot weken of kunnen het lange termijn gedrag van breedte–gemiddelde grootheden geven (Fokkink, 1998; De Jong, 1998). Het is bijvoorbeeld nog niet mogelijk om het drie dimensionale gedrag van geulen en platen te simuleren over een periode van maanden tot jaren.

Deze problematiek vormt het algemene kader van het huidige onderzoeksproject, dat wordt uitgevoerd in opdracht van het RIKZ Middelburg door het IMAU (universiteit Utrecht). De nadruk ligt hierbij op een specifiek estuarium, namelijk de Westerschelde, zie figuur 1. Dit bekken is economisch van groot belang omdat het de scheepvaartroute naar de haven van Antwerpen is. Daarnaast heeft het gebied een grote ecologische waarde. Uitgangspunt van het beheer is het garanderen van de scheepvaart met behoud van de natuurlijke waarde van het estuarium. De afgelopen jaren heeft dit tot problemen geleid: baggeractiviteiten (zo'n 8×10^6 m^3/jr) en verdieping van de vaargeul hebben gezorgd voor verminderde activiteit van geulen en platen in het bekken; de vraag vanuit het beheer is of en hoe deze negatieve effecten kunnen worden voorkomen.

De doelstellingen van dit onderzoek zijn

- het vaststellen of er morfodynamische evenwichten bestaan;
- het bekijken van de stabiliteit van deze evenwichten;
- het lange termijngedrag van geulen en platenstelsels bestuderen;
- het onderzoeken van de gevoeligheid van evenwichten op ingrepen;

Teneinde deze vragen te beantwoorden wordt er een geïdealiseerd model ontwikkeld en bestudeerd. Dit model bevat de essentiële fysica en is bedoeld om meer fundamentele kennis te verkrijgen van de morfodynamica van getijdebekkens.

De Westerschelde

De totale lengte van de Westerschelde bedraagt zo'n 160km (tot Gent); in het mariene gedeelte (de eerste 60 km) neemt de breedte van het bekken langzaam af van 5km naar enkele honderden meters. Waterdiepten in de geulen variëren van 25m nabij Vlissingen tot 50m nabij Borssele en nemen dan af richting Antwerpen. De waterbeweging in het bekken wordt gedomineerd door het dubbeldaagse zon– en maansgetij; de amplitude van de waterstanden bedraagt ongeveer 2m nabij Vlissingen en neemt het bekken in toe ($\pm$ 2.5m nabij Antwerpen), karakteristieke stroomsnelheidsamplituden bedragen ongeveer 1m/s. De waargenomen faseverschuiving in landwaartse richting duidt op een gedeeltelijk gereflecteerde getijgolf. Ten gevolge van de traagheid van de waterbeweging, bodemwrijving en massabehoud worden hogere harmonischen van het basisgetij opgewekt (met name de M_4-component en in mindere mate de M_6 component), alsmede residuele stromingen. Dit resulteert in intern gegenereerde asymmetrie van zowel het vertikale- als het horizontale getij. Daarnaast bestaat er ook extern opgelegde asymmetrie als gevolg van de door de Noordzee opgelegde M_2- en M_4-getijcomponenten aan de zeewaartse rand van het bekken. De uitstroom van de Schelderivier bedraagt gemiddeld 100 m^3/s, hetgeen klein is ten opzichte van de getijfluxen (ongeveer 1% op de Nederlands–Belgische grens).

De door de waterbeweging geïnduceerde bodemschuifspanningen zijn voldoende groot om sediment op te wervelen en te transporteren. Het grootste gedeelte van het materiaal bestaat uit fijn zand (korrelgrootte ongeveer 0.2 mm), dat wordt getransporteerd als zwevend stof. Ten gevolge van met name getijasymmetrie, reststromingen en 'settling lag' effecten ontstaan netto transporten, die bepalend zijn voor de morfologie. Met settling lag wordt bedoeld dat er een faseverschil is tussen de concentratie van gesuspendeerd materiaal en de stroomsnelheid omdat deeltjes enige tijd nodig hebben om uit te zakken.

De morfologie van de Westerschelde wordt gekenmerkt door een aantal hoofdgeulen, waarvan het aantal afneemt van drie aan de zeewaartse zijde tot 1 dieper in het bekken. Er blijkt een duidelijk verschil tussen ebgeulen (getijgemiddeld transport van water zeewaarts gericht) en vloedgeulen. De eerstgenoemden vertonen meandergedrag, met een kenmerkende lengteschaal van 5km, terwijl de laatsten meer recht zijn. Op de overgang tussen twee bochten bevinden zich drempels, dat wil zeggen locaties waar netto sedimentatie optreedt. De hoofdgeulen zijn onderling verbonden door zogeheten kortsluitgeulen, die cyclisch gedrag blijken te vertonen in ruimte en tijd. Verder worden in bepaalde gebieden van het bekken, zoals in het Verdronken Land van Saaftinghe, fractale patronen van geulen waargenomen.

Het model

Teneinde de fundamentele kennis van het morfologische gedrag van de Westerschelde te vergroten is een geïdealiseerd model van dit bekken ontwikkeld. Een groot voordeel van zo'n model is dat slechts een beperkt aantal fysische processen expliciet wordt beschreven, zodat het transparant is en kan worden geanalyseerd met behulp van wiskundige methoden. Vergelijkbare modellen zijn hiervoor ontwikkeld voor de korte bekkens in de Waddenzee (lengte veel korter dan de getijgolflengte) en zijn zeer succesvol omdat ze een verklaring gaven voor waargenomen gedrag. Voorbeelden zijn de geobserveerde bodemprofielen, bekende empirische relaties (zoals een ruimtelijk uniforme bodemschuifspanning), het netto importeren van sediment na een gedeeltelijke afsluiting (Friese Zeegat), het ontstaan en splitsen van geulen en het migratiegedrag van platen aan de zeewaartse kant van de bekkens.

Het model voor de Westerschelde verschilt op een aantal wezenlijke punten van die voor korte bekkens. In de eerste plaats betreft het hier een lang bekken, zodat er sprake is van een ruimtelijk niet-uniforme getij. Dit heeft tevens als consequentie dat bodemwrijving een cruciale rol speelt in de dynamica van de waterbeweging. Tevens is de rol van traagheid essentiëel, waardoor getij-asymmetrie en reststromen ontstaan en het dominante transport van sediment op de getijdetijdschaal wordt bepaald door advectieve processen. Aangezien korte bekkens het bestaan van morfologische evenwichten toelaten is als eerste onderzocht of het Westerscheldemodel morfodynamische evenwichten toelaat en hoe deze afhangen van de parameters. Ten tweede zijn de stabiliteitseigenschappen van deze evenwichten onderzocht teneinde na te gaan of geulen/platen als vrije instabiliteit van een gekoppeld water–bodemsysteem kunnen ontstaan.

Het domein van het model is een rechthoekig bekken met niet-erodeerbare zijwanden en aan de landwaartse zijde is de waterdiepte nihil, zie figuur 2. De bewegingsvergelijkingen bestaan uit de dieptegemiddelde ondiepwatervergelijkingen, waarin de bodemschuifspanning is gelineariseerd volgens het Lorentz-principe. Daaraan zijn toegevoegd een vergelijking voor de breedtegemiddelde- en dieptegeïntegreerde concentratie, inclusief opwerveling- en depositietermen, en een bodemevolutievergelijking. Als randvoorwaarden wordt op de zeewaartse rand het vertikale getij voorgeschreven (zowel een M_2- als M_4-component) en de bodem vastgehouden. Aan de landwaartse kant wordt de netto sedimentflux (bestaande uit een advectief en diffusief deel) nul gesteld. Tot slot worden geen diffusieve grenslagen in het tijdoscillerende deel van de concentratie toegestaan. Het eerste belangrijke verschil met een eerder model, ontwikkeld door Karin de Jong, is dat hier geen rivieruitstroom wordt meegenomen. In plaats daarvan kunnen advectieve fluxen worden gecompenseerd door diffusieve fluxen, waardoor wel grenslagen in de gemiddelde concentratie ontstaan. Een tweede verschil is dat hier intern gegenereerde getij-asymmetrie expliciet wordt meegenomen; in het model van de Jong is er alleen sprake van extern opgelegde getij-asymmetrie. Tot slot wordt in het hier besproken model de dwarsdoorsnede van het bekken constant verondersteld, terwijl dit in het andere model ruimtelijk variëert. Teneinde de modellen op dit punt te kunnen vergelijken kan, bij een gegeven modelbodem, een actuele dwarsdoorsnede worden berekend door de waterdiepte te vermenigvuldigen met de actuele breedte.

Analyse en resultaten

Het model is allereerst dimensieloos gemaakt door gebruik te maken van relevante ruimte- en tijdschalen. Belangrijk daarbij is dat de morfologische tijdschaal veel groter is dan de getijperiode en wrijvingstijdschaal. Dit leidt tot een dimensieloze wrijvingscoëfficiënt, die evenredig is met de bekkenlengte.

Vervolgens is het model geanalyseerd door een ontwikkeling te maken in twee kleine parameters, namelijk ϵ en β. De eerstgenoemde geeft de verhouding van de vertikale getij-amplitudo en de waterdiepte op de zeewaartse rand, de tweede de amplitudeverhouding van het M_4- en M_2-getij op de open rand. De overige belangrijke modelparameters zijn de fase van het M_4-getij op de open rand, de bodemwrijvingscoëfficiënt en de lengte van het bekken. Vooralsnog is alleen gezocht naar morfodynamische evenwichten, die gekenmerkt worden door de afwezigheid van een netto sedimentflux in het gehele bekken. De oplossingen zijn berekend met behulp van continuatietechnieken, dat wil zeggen uitgaande van bekende oplossingen (in de korte bekkenlimiet) worden oplossingen geconstrueerd door bepaalde parameters (bekkenlengte, sterkte van het externe M_4-getij, etc.) geleidelijk te veranderen.

Allereerst is de situatie onderzocht waarbij er geen extern opgelegde hogere harmonischen van het basisgetij werden beschouwd, d.w.z. parameter $\beta = 0$. De resultaten zijn weergegeven in figuur 4, voor een discussie van de parameters in deze figuur, zie secties 2 en 3. Alle overige parameters zijn zodanig gekozen dat ze representatief zijn voor de Westerschelde. Opvallende kenmerken zijn dat in het korte bekkenregime het bodemprofiel een nagenoeg constante helling heeft. Voor toenemende bekkenlengte wordt dit profiel steeds meer concaaf, als gevolg van traagheids- en continuiteitseffecten en de toenemende invloed van bodemwrijving. Als de bekkenlengte ongeveer een kwart is van de wrijvingsloze getijgolflengte treedt er resonantie op van het M_2-getij. Voor nog grotere bekkenlengten ontstaat een bodemprofiel waarbij vanaf de zeewaartse rand de waterdieptes eerst toenemen en pas achterin flink afnemen. Dit laatste hangt samen met de opwekking van een sterk M_4-horizontaal getij achterin het bekken als gevolg van bodemwrijving. Teneinde de daarmee samenhangende netto transporten te neutraliseren krijgt de bodem achterin het bekken een convex profiel. De getijgolf verandert qua karakter steeds meer van een staande golf naar een lopend golf. Voor een bekkenlengte groter dan de wrijvingslengteschaal van het bekken (deze wrijvingslengte hangt af van de gekozen parameters) bestaat er geen morfodynamisch evenwicht meer. De conclusies zijn dus dat ook lange bekkens morfodynamische evenwichten hebben en dat ze bij afwezigheid van externe overtides uniek zijn. Echter voor bekkenlengten groter dan de wrijvingslengteschaal van de getijgolf bestaan geen evenwichten meer.

Het toelaten van externe overtides in het model leidt tot wezenlijke nieuwe verschijnselen. Dit komt omdat naast het M_2-getij ook het externe M_4-getij resonantiegedrag vertoont. Vooralsnog is alleen het geval onderzocht waarbij het faseverschil tussen de twee getijcomponenten op de zeewaartse rand 0 graden is, zoals het geval is bij de Westerschelde. Voor relatief korte bekkenlengten zijn sedimentfluxen geïnduceerd door externe overtides veel groter dan degene die bepaald worden door intern gegenereerde overtides. Als gevolg hiervan hebben deze evenwichten significant andere kenmerken, zie sectie 5.2. De waterdiepten nemen vanaf de zeewaartse rand naar binnen sterk toe en bereiken een maximum ongeveer halverwege het bekken. De maximale waterdiepte wordt bereikt bij een bekkenlengte van ongeveer 75km en bedraagt, in het geval van de Westerschelde, meer dan 30m. De bijbehorende getijgolf blijkt vooral een staand karakter te hebben. Dit evenwicht kan echter niet langer bestaan voor lengten groter dan 75km, hetgeen de wrijvingslengteschaal van het externe M_4-getij is.

Interessant is dat er voor bekkenlengten groter dan 135km nog evenwichten kunnen bestaan, die qua eigenschappen sterk overeenkomen met de evenwichten die hiervoor zijn beschreven. Deze bestaan in het geval $\beta = 0.07$, hetgeen representatief is voor de Westerschelde, voor bekkenlengten tussen de 75 en 135km. Als de sterkte van het externe M_4 getij wordt vergroot ($\beta > 0.12$) kunnen deze twee typen evenwichten bestaan voor dezelfde parameterwaarden. Het eerste type evenwicht wordt bepaald door een balans tussen sedimentfluxen die geïnduceerd worden door extern geforceerde getijasymmetrie; het tweede type evenwicht is gerelateerd aan interne getij-asymmetrie. Voor afnemende waarden van β zijn deze evenwichten steeds minder van elkaar te onderscheiden en vloeien uiteindelijk samen.

Vervolgens zijn de wateruitwijkingen en het bodemprofiel van het morfodynamisch evenwicht zoals gevonden met behulp van bovenstaande analyse vergeleken met waarnemingen. Gezien de vele vereenvoudigingen gebruikt in het model komen de gevonden waterstanden, fase-verschuivingen en bodemvormen redelijk goed overeen met de waarnemingen. Vooral de fase van het M_2 en M_4 vertikaal getij worden goed gereproduceerd door het model. De amplitude van het vertikale M_2 getij bij Antwerpen (waar resonantie optreedt) wordt enigszins onderschat. Dit kan echter worden verbeterd door convergentie van het bekken toe te voegen.

Het bestaan van meerdere evenwichten en de bijbehorende stabiliteitseigeschappen kan belangrijke consequenties hebben voor het beheer van getijdebekkens. Teneinde dit te onderzoeken is een numeriek model geconstrueerd dat de tijdsontwikkeling van bodemprofielen, en de daaraan gekoppelde waterbeweging en sedimentfluxen, beschrijft. Het blijkt dat zelfs voor grote bodemverstoringen het systeem telkens evolueert naar het oorspronkelijke evenwicht.

Verder is de stabiliteit van twee-dimensionale verstoringen op de gevonden één dimensionale evenwichten bestudeerd. Deze verstoringen vertonen structuren die vergeleken kunnen worden met de geul–plaat structuren zoals waargenomen in veel estuaria. Uit deze lineaire stabiliteitsanalyse volgt dat, als de wrijvingscoëfficient groot genoeg is, het één-dimensionale evenwichtsprofiel instabiel wordt en er twee dimensionale bodemvormen ontstaan. Echter, aangezien de analyse een lineaire stabiliteitsanalyse is, wordt alleen de initiële groei van deze structuren beschreven. Om het eindige-amplitude gedrag te kunnen beschrijven moet het volledige niet–lineaire model worden gebruikt. Hieraan zal in fase drie worden gewerkt.

1 Introduction

In many tidal inlets and estuaries a dynamic interaction between the water motion and the morphology is observed. This usually results in a complex pattern of channels and shoals, see e.g. the Western Scheldt (Van den Berg *et al.*, 1990). This estuary is located in the the south–west of Holland and Belgium and serves as the main navigation lane to the harbour of Antwerp (see figure 1). In the Western

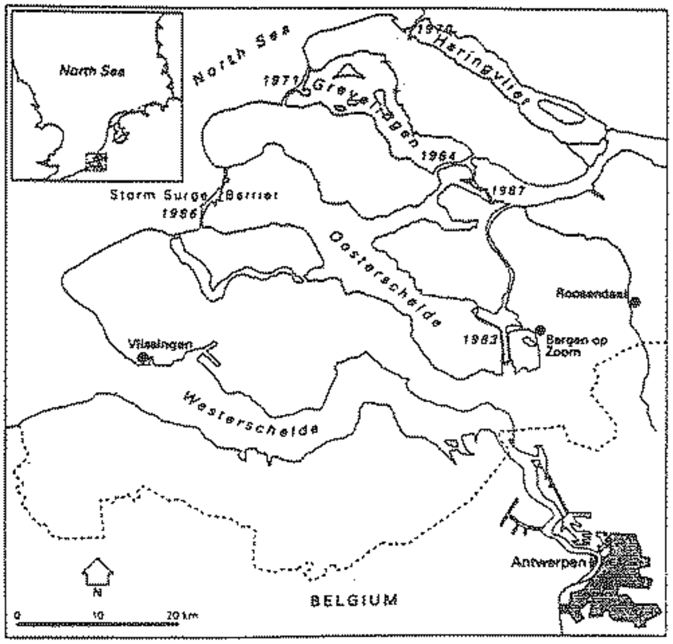

Figure 1: The marine salt and brackish part of the Western Scheldt estuary from Vlissingen to Antwerp.

Scheldt economical and ecological interests often interfere. For shipping purposes it would be advantageous if the channel was canalized. On the other hand, the Western Scheldt has important feeding grounds for birds and other animals for which the system has to be kept as dynamic as possible. To keep the harbour open for large ships, the navigation lane of the Western Scheldt has to be dredged continuously $(8 \cdot 10^6 \; \mathrm{m}^3 \mathrm{year}^{-1})$ (Verbeek *et al.*, 1998). Since the morphology is also very sensitive to changes in exogenous conditions (see Van der Spek (1997)) our understanding of the estuarine processes must be deepened to be able to manage and control the changes in these complex systems. In recent years there has been considerable progress in the modelling of morphological phenomena in tidal inlet systems using process–oriented models (see Wang *et al.* (1995); De Vriend & Ribberink (1996)). However, there are still open problems with regard to an accurate simulation of sediment transport patterns and morphologic developments. Thoolen & Wang (1999) demonstrated this explicitely for the Western Scheldt estuary and concluded that discrepancies are mainly due to a lack of process knowledge. This motivates the development of idealized models, in which specific processes can be studied in isolation and which are simpler to analyze. Their results will give clues as to how to interpret both field data and the results of more complex models.

The main objective of the present project is to gain more fundamental knowledge about the morphodynamic behaviour of the Western Scheldt estuary and in particular about the dynamics of channels and shoals. This will be done by development and analyzis of an idealized model for an embayment which has the characteristics of the Western Scheldt. The model is based on the depth–integrated shallow water equations, supplemented with a suspended sediment transport module and a bottom evolution equation. The procedure is to study first the existence of morphodynamic equilibria which have no structure in the cross–channel direction. The motivation for this approach is that channels and shoals often develop as an inherent instability of a one dimensional morphodynamic equilibrium (see Schielen *et al.* (1993); Seminara & Tubino (1997); Schuttelaars (1999)). First results with respect to one–dimensional were discussed by Schuttelaars (to appear); Schuttelaars & De Swart (1999, submitted). The important extension with respect to previous work (Schuttelaars & De Swart, 1996) is that the embayment length is not a priori considered to be short with respect to the tidal wave–length. That implies that the new model can also be applied to systems like the Western Scheldt. The implications of an unconstrained embayment length are that the spatial variations of both the vertical and horizontal tide due to inertial and frictional effects. This results in the possibility of tidla resonance and additional tidal asymmetry with important consequences fot the sediment transport. Furthermore, in a long channel the net transport of suspended sediment is mainly due to advection, whereas in a short embayment the main transport mechanism is diffusive transport. Important differences with De Jong (1998) are the neglect of river influence and the incorporation of diffusive boundary layers in the averaged concentration equation. An important result is that morphodynamic equilibria exist for embayment lengths smaller than a maximum length which is related to the frictional length scale of the tide. Moreover, for realistic values of the parameters the existence of multiple morphodynamic equilibria was demonstrated.

In this report the emphasis is on three aspects. First, a detailed comparison is made between model predictions and field observations in the Western Scheldt with regard to one dimensional morphodynamic equilibria. Secondly, the stability of these equilibria is studied by introducing a perturbation in the bed and following the bed evolution in time. Lastly, the stability properties of these equilibria with respect to bottom perturbations with a cross–channel structure will be investigated and the sensitivity with respect to model parameters will be analyzed.

In section 2 the model will be presented, in section 3 the equations are scaled and analyzed using an asymptotic method. In section 4 one–dimensional morphodynamic equilibria and their characteristics will be studied. Furthermore, a comparison with observations is made. In section 5 the linear stability of the one–dimensional equilibria will be studied. In the last section some conclusions and suggestions for future work will be made.

The contents of the paper is as follows. In section 2 the model will be presented, whereas in section 3 the equations are scaled and analyzed using an asymptotic method. The short embayment regime is studied in section 4 and new results are obtained since finite embayment lengths are considered. The characteristics of morphodynamic equilibria for longer embayment lengths are discussed and interpreted in section 5. In section 6 the model results are compared with field data, while in section 7 the time evolution of perturbed beds is shown. In section 8 the linear stability of the one dimensional equilibria is studied and we end with the conclusions.

2 Model Description

The embayments under study are rectangular, i.e. width variations are neglected. The water motion is forced at the seaward entrance by a prescribed sea surface variation ζ of tidal origin, see figure 2. The boundary on the landward side is assumed to be closed, hence effects of river outflow are not included and the water density can be taken as constant. This is a good approximation for many embayments, e.g. in case of the Western Scheldt the river discharge at the Dutch-Belgium border is less than one percent of the tidal prism (Van den Berg *et al.*, 1990). Moreover, the water depth at the landward boundary is assumed to vanish, thereby allowing a finite velocity at this location. The latter is a necessary condition for the presence of morphodynamic equilibria in such systems, as was already demonstrated for short tidal channels by Schuttelaars & De Swart (1996). Note that due to free surface elevations the boundary at the landward side is a *moving* boundary (see figure 2, where the lengths corresponding to sea level states ζ_1 and ζ_2 are L_1 and L_2, respectively). The reference undisturbed water depth is denoted by H, the bed elevation by h and u is the horizontal tide.

The embayment width is considered to be much larger than the reference water depth, but to be much smaller than both its length and the Rossby deformation radius. This implies that the water motion can be described by the cross–sectionally

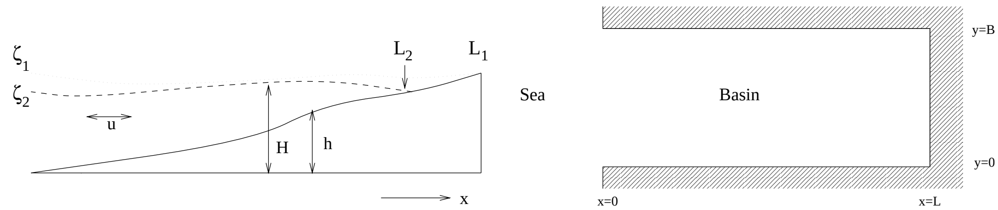

(a) (b)

Figure 2: Topview and side view of the embayment. For explanation of the symbols see the text.

averaged shallow water equations for a homogenous fluid:

$$\zeta_t + [(H - h + \zeta)u]_x = 0 \tag{1a}$$

$$u_t + uu_x + g\zeta_x + \hat{r}\frac{u}{H - h + \zeta} = 0 \tag{1b}$$

Here subscript defines differentiation with respect to that variable unless stated differently. Furthermore, $\hat{r} = 8UC_{\mathrm{D}}/3\pi$, with U is a characteristic velocity scale and $C_{\mathrm{D}} \sim 0.001$ the drag coefficient. The bottom friction in the momentum equation (1b) is linearized according to the energy dissipation condition discussed in Zimmerman (1992). The boundary conditions have already been discussed.

The sediment in the embayment consists of noncohesive material with only one grain size and is mainly transported as suspended load. This transport is described by a depth–integrated concentration equation (see Van Rijn (1993)):

$$[C_t + (uC - \mu_\star C_x)_x] = \alpha u^2 - \gamma C \tag{2}$$

Here C is the depth–integrated sediment concentration, *i.e.*, the amount of sediment stored in a column sea water with unit horizontal area and $\mu_\star$ is a constant diffusion coefficient of order $100\,\mathrm{m}^2\mathrm{s}^{-1}$. The sedimentation at the top of the active layer consists of the whirling up and settling of sediment. The sediment pick–up function is parametrized as αu^2, where α is a coefficient related to sediment properties (grain size, shape, etc.). This parameterization is motivated by the analysis of field observations reported by Dyer & Soulsby (1988). Typically, $\alpha \sim 3 \times 10^{-2}$ kgsm^{-4} for fine sand with a grainsize of 2×10^{-4} m. The term $-\gamma C$ models the deposition of the sediment. The constant γ can be related to the settling velocity and a diffusion coefficient κ_{v} that describes the mixing of the sediment in the vertical. Assuming a constant κ_{v} it follows from Van Rijn (1993) that $\gamma = u_{\mathrm{s}}^2/\kappa_{\mathrm{v}} \sim 4 \times 10^{-3}\,\mathrm{s}^{-1}$ for fine sand.

One of the boundary conditions for the concentration equation is that the tidally averaged sediment flux is zero at the time-mean position of the landward boundary. At the entrance it is imposed that the bed does not change. Since the bed only changes due to tidally averaged erosion and deposition, additional conditions are needed to determine the variations of the concentration on the tidal timescale. Here it is imposed that no diffusive boundary layers develop in the fluctuating part of the concentration.

The bottom evolution equation is derived from continuity of mass in the sediment layer and reads

$$\rho_{\mathrm{s}}(1-p)h_t = -\left\langle \alpha u^2 - \gamma C \right\rangle \tag{3}$$

where $< . >$ denotes an average over the tidal period, $p(\sim 0.4)$ the bed porosity and $\rho_{\mathrm{s}}(\sim 2650\,\mathrm{kgm}^{-3})$ the density of the individual grain particles. Since at $x=0$ the total deposition equals the erosion, the bed remains fixed at $x=0$, at the end the water depth is always zero.

3 Scaling and Expansion

The equations as discussed in section 2 are scaled using

$$\begin{aligned} x &= L\tilde{x}, \qquad t = \tilde{t}\sigma^{-1}, \qquad u = \frac{A\sigma L}{H}\tilde{u} \\ \zeta &= A\tilde{\zeta}, \qquad h = H\tilde{h}, \qquad C = \frac{\alpha U^2}{\gamma}\tilde{C} \end{aligned} \tag{4}$$

Here L is chosen such that $x=1$ is the intersection point of the bed profile and the undisturbed water level. The radian frequency of the main tidal constituent is denoted by σ and A is the amplitude of the vertical tide at the entrance. Suppressing the tildes, the dimensionless equations read

$$\zeta_t + [(1-h+\epsilon\zeta)u]_x = 0 \tag{5a}$$

$$u_t + \epsilon u u_x + \lambda^{-2}\zeta_x + r\frac{u}{1-(h-\epsilon\zeta)} = 0 \tag{5b}$$

$$a\left[C_t + (\epsilon u C - \mu C_x)_x\right] = u^2 - C \tag{5c}$$

$$h_\tau = -\left\langle u^2 - C \right\rangle \tag{5d}$$

Here ϵ is, apart from a factor of 2π, the ratio of the tidal excursion (the distance travelled by a fluid particle in a tidal period) and the embayment length (for the definitions of the nondimensional parameters in the model, see table 1).

Parameters in the nondimensional model		
$\epsilon = \frac{A}{H} = \frac{U}{\sigma L}$	$\lambda = \frac{\sigma L}{\sqrt{gH}} = \frac{2\pi L}{L_{\mathrm{g}}}$	$r = \frac{8C_{\mathrm{D}}AL}{3\pi H^2}$
$a = \frac{\sigma}{\gamma}$	$\mu = \frac{\mu_\star}{\sigma L^2}$	$\delta = \frac{\alpha U^2}{\rho_{\mathrm{s}}(1-p)H\sigma}$

Table 1: Parameter definitions in the nondimensional model.

The constant λ is, apart from a factor of 2π, the ratio of the embayment length and the frictionless tidal wave length L_{g}, and r is the bottom friction parameter. Furthermore, a is the ratio of the timescale of the deposition process and the tidal period and μ is the ratio of the tidal period and the diffusive time scale. Here $\tau = \delta t$ is a slow time coordinate.

Note that in (5b) the friction term becomes singular for vanishing water depths. To avoid this unphysical behaviour the depth $h - \epsilon\zeta$ of the water column is multiplied by a parameter having a value close to 1.

The bottom evolution equation can also be written as

$$h_\tau = -F_x \qquad\qquad F = a < \epsilon u C - \mu C_x > \tag{6}$$

as follows from subsituting the concentration equation 5c in 5d. Hence the bottom changes are determined by the divergence of a net sediment flux F, which consists of an advective and diffusive part, respectively.

The boundary conditions at the entrance $x = 0$ are

$$\zeta = \cos(t) + \beta\cos(2t - \phi) \tag{7a}$$
$$h = 0 \tag{7b}$$
$$C'(x, t, \mu) = C'(x, t, \mu = 0) \tag{7c}$$

Here β is the ratio of the M_4 amplitude and the M_2 amplitude at the entrance, ϕ is the phase difference between the M_4 and M_2 tidal constituents at this location, defined by $\phi = \phi_{M_4} - 2\phi_{M_2}$. At the closed end the boundary conditions read

$$u_x \quad \text{is finite} \tag{8a}$$
$$\langle \epsilon u C - \mu C_x \rangle = 0 \tag{8b}$$
$$C'(x, t, \mu) = C'(x, t, \mu = 0) \tag{8c}$$

Note that the conditions, which were originally formulated at the moving landward boundary, have been transformed to conditions at the fixed boundary $x = 1$. This has been done by using Taylor expansions, where it has been used that the maximum horizontal displacement of the landward boundary during a tidal cycle is small compared with the mean embayment length. Here C' is the oscillatory part of the concentration equation. The first boundary condition is the kinematic boundary condition, the second one states that no net sediment flux is allowed through $x = 1$. The conditions (7c) and (8c) state that no diffusive boundary layers develop in the time-varying part of the concentration near the entrance and the landward side of the embayment.

These equations are solved by making an expansion with respect to the small parameters ϵ and β, up to first order. Hence it is assumed that both $\epsilon \ll 1$ and $\beta \ll 1$, but their ratio is not prescribed. The condition on β implies that the M_2 constituent is much stronger than the externally prescribed M_4 constituent. Hence the following expansions are made:

$$\Psi = \Psi_0 + \epsilon\Psi_1 + \beta\hat{\Psi}_1 \ldots \tag{9}$$

with

$$\Psi_0 = \Psi^{\mathrm{s}} \sin(t) + \Psi^{\mathrm{c}} \cos(t) \tag{10a}$$

$$\Psi_1 =< \Psi > + \Psi^{2\mathrm{s}} \sin(2t) + \Psi^{2\mathrm{c}} \cos(2t) \tag{10b}$$

$$\hat{\Psi}_1 = \hat{\Psi}^{2\mathrm{s}} \sin(2t) + \hat{\Psi}^{2\mathrm{s}} \cos(2t) \tag{10c}$$

where Ψ is any of the variables ζ, u and C'. The component Ψ_0 decribes the main tidal constituent and $< \Psi >$ the mean contributions generated by nonlinear interactions. Note that by definition $< C' >= 0$. Furthermore $\Psi^{2\mathrm{c}}, \Psi^{2\mathrm{s}}$ are the internally generated M_4 overtide and $\hat{\Psi}^{2\mathrm{s}}, \hat{\Psi}^{2\mathrm{c}}$ the M_4 overtide components generated by external forcing. Superscripts are used to describe the temporal behaviour on the short time scale. Of course, one can write $\zeta_0 = |\zeta_0| \cos(t - \phi_{\zeta_0})$, etc., as well. Here $|\zeta_0|$ is the amplitude of the M_2 vertical tidal elevation and ϕ_{ζ_0} its phase angle.

If a bed profile and the surface elevations at the entrance of the embayment are given, the horizontal and vertical velocities and the concentration can be calculated explicitely. This information is used to calculate a net sediment flux F. Now from 6 it is clear that a morphodynamic equilibrium is defined by $h_\tau = 0$. Using the boundary condition (8b), this means that in equilibrium the net sediment flux throughout the embayment has to be zero. In terms of the tidal components defined in (10a) this condition reads

$$\begin{aligned} F = -a\mu < C >_x + a\epsilon^2 \Big(& < u >< C > \\ & + \frac{1}{2} \left[u^{\mathrm{s}} C^{\mathrm{s}} + u^{\mathrm{c}} C^{\mathrm{c}} + u^{2\mathrm{s}} C^{2\mathrm{s}} + u^{2\mathrm{c}} C^{2\mathrm{c}} \right] \Big) \\ & + a\frac{1}{2}\epsilon\beta \left(u^{\mathrm{s}} \hat{C}^{\mathrm{s}} + u^{\mathrm{c}} \hat{C}^{\mathrm{c}} + \hat{u}^{2\mathrm{s}} C^{2\mathrm{s}} + \hat{u}^{2\mathrm{c}} C^{2\mathrm{c}} \right) = 0 \end{aligned} \tag{11}$$

Note that the net sediment flux consists of different contributions. The first term on the r.h.s. is the diffusive flux. The term proportional to $a\epsilon^2$ contains advective fluxes which are due to velocity and concentration components induced by internal nonlinear interactions. On the last line all advective fluxes are collected which are caused by the presence of external overtides. So if an equilibrium bed profile is obtained, the combination of the velocity and concentration fields as given in (11) is such that the total time–averaged flux is zero. Using the knowledge of the equilibrium solution in case of the short embayment limit (see Schuttelaars & De Swart (1996)) and standard numerical methods (continuation techniques in slowly varying parameters), equilibrium bed profiles and their corresponding velocity fields, surface elevations and concentration fields for different embayment lenghts, tidal forcing etc. can be obtained.

4 Results for short embayments

In this section the case that $\lambda \equiv 2\pi L/L_{\rm g} \ll 1, r = \mathcal{O}(1)$ is considered, i.e., the embayment length is much shorter than the tidal wave–length. This moderate dissipative regime was also studied by Schuttelaars & De Swart (1996), but an important difference is that here, instead of taking the limit $\lambda \to 0$, the effects of small but finite values of λ will be considered. Results will be shown for parameter values which are representative for the Frisian Inlet, a short embayment located in the Dutch Wadden Sea. The parameter values presented in table 2 are extracted from Van de Kreeke & Dunsbergen (to appear); Wang *et al.* (1995) and references herein.

Quantities in the dimensional model		
$H \sim 10$ m	$L \sim 2 \cdot 10^4$ m	$\sigma \sim 1.4 \cdot 10^{-4}$ s^{-1}
$A \sim 1.0$ m	$\mu_\star \sim 10^2$ m^2 s^{-1}	$C_{\rm D} \sim 1 \cdot 10^{-3}$
Parameters in the nondimensional model		
$\epsilon \sim 0.15$	$a \sim 0.04$	$\mu \sim 1.8 \cdot 10^{-3}$
$\delta \sim 2.4 \cdot 10^{-3}$	$\lambda^2 \sim 0.078$	$r \sim 0.25$
$\beta \sim 0.08$	$\phi \sim 7^\circ$	

Table 2: Quantities and parameter values for the Frisian inlet system.

In Schuttelaars & De Swart (1996) it was found that if external overtides in the forcing at the entrance are neglected (i.e., parameter $\beta = 0$) then the model has a unique one–dimensional stable morphodynamic equilibrium. The latter describes a spatially uniform tidal current over a constantly sloping bottom with a vanishing depth at the landward boundary, see the dashed curve in figure 3. The equilibrium bottom profile, obtained with the present model in the short embayment regime, is shown in the same figure by the solid curve. From this it appears that the effect of small $\mathcal{O}(\lambda^2)$ contributions causes the equilibrium bottom profile to become concave.

The behaviour observed in figure 3 can be understood as follows. First con-

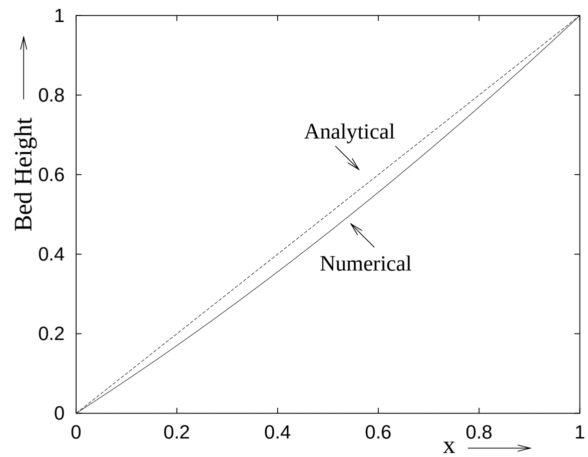

Figure 3: Analytical (no λ^2 corrections) and numerical equilibrium bottom profiles (scaled with reference depth H) versus the dimensionless distance to the seaward boundary (scaled with embayment length L; in this case $L = 2 \cdot 10^4$ m). The other parameter values are given in table 2.

sider the model in the limit $\epsilon \to 0$, i.e., nonlinear contributions are neglected. This implies that the net sediment flux, defined in (11), is fully determined by the diffusive contribution. In this case a morphodynamic equilibrium is characterized by $< C >_x = 0$, which implies a spatially uniform time-mean depth-integrated concentration. The latter follows from the tidally averaged concentration equation 5c and reads $< C > \simeq < u^2 >$. Here it has been used that $a \ll 1$, i.e., the deposition timescale is much smaller than the tidal period. An approximate result for the velocity field can be obtained from substitution in 5a – 5b of perturbation series for u and ζ in powers of the small parameter λ. Now assume that the bottom profile is $h = x$, which has a constant slope. Then it appears that

$$
\begin{aligned}
u &= u^{\mathrm{s}} \sin t + u^{\mathrm{c}} \cos t \\
u^{\mathrm{s}} &= -\left[1 + \frac{1}{2}\lambda^2(1+x)\right], \quad u^{\mathrm{c}} = \mathcal{O}(\lambda^2)
\end{aligned}
\tag{12}
$$

Quantities in the model		
$H = 10$ m	$A = 1.75$ m	$\sigma \sim 1.4 \cdot 10^{-4}$ s^{-1}
$\mu_\star = 10^2$ m^2 s^{-1}	$a = 0.01$	$C_\mathrm{D} = 1 \cdot 10^{-3}$
$\beta \sim 0.074$	$\phi \sim 1^\circ$	

Table 3: Quantities and parameter values used in the numerical experiments with variable embayment length. They are representative for the Western Scheldt

Clearly $< u^2 >$ increases towards the landward boundary, which is due to tidal resonance effects. Consequently also $< C >$ increases towards the land which means that $h = x$ is not a steady bottom profile. In fact diffusive fluxes will occur and cause a net export of sediment, resulting in a concave equilibrium bottom profile. This argument still applies in case that nonlinear terms are retained, because in the short embayment regime advective sediment fluxes behave in a similar way as the diffusive flux (Schuttelaars & De Swart, 1996).

The introduction of overtides in the forcing ($\beta > 0$) resulted in more complex dynamics. First consider the case that the phase shift between the external M_2 and M_4 tide at the entrance is $\phi = 0$. This situation is representative for most Dutch tidal inlet systems. Then embayments with λ small but finite have equilibrium bed profiles which are even more concave than in case $\beta = 0$. This follows directly from an analysis similar to the one which resulted in (12). For phase shifts $\phi < 0$ even more concave bottom profiles are found, for $\phi > 0$ the profile tends to become convex.

5 Results for embayments with arbitrary lengths

In the numerical experiments, the influence of different parameter values on the maximum embayment length and the number of possible morphodynamic equilibria was investigated. One of the most interesting questions is whether one or more morphodynamic equilibria exist for all embayment lengths, given a set of parameters. Usually the length was varied with all other parameters kept constant. The default values used in the experiments are given in table 3 and are representative for a long tidal embayment such as the Western Scheldt estuary (see Van den Berg *et al.* (1990); De Jong (1998)).

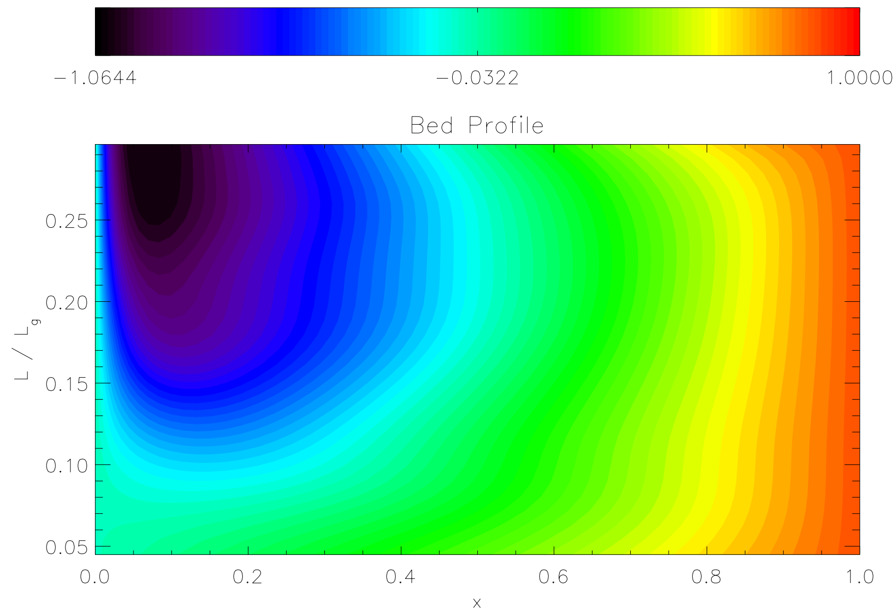

Figure 4: Contour plot of the equilibrium bed level h (scaled with water depth H) as a function of the dimensionless coordinate x and the length scale ratio L/L_{g}. The system is only driven by an externally prescribed M_2 tide ($\beta = 0$). Other parameter values are given in table 3. Here L_{g} is the frictionless tidal wave-length, in this case $L_{\mathrm{g}} \sim 450$ km.

5.1 No Overtides

In this series of experiments the embayment length was varied under the assumption that the system is only driven by an externally prescribed M_2 constituent ($\beta = 0$). Thus overtides are only generated internally by nonlinear interactions. Note that due to variation of the embayment length the scaled diffusion constant $\mu = \mu_\star/\sigma L^2$, the friction coefficient r and the ratio δ of the tidal period and the morphological timescale change. This means that the relative importance of advective sediment fluxes (which scale with ϵ^2) over diffusive fluxes become more important with increasing L.

In plate 4 a contour plot is shown of the equilibrium bed profile h (for its definition, see figure 2), scaled by reference depth H, as a function of the dimensionless coordinate x (distance from the seaward boundary, scaled by the length L) and parameter L/L_{g}. Here $L_g = \sqrt{gH}\,T$ (T is the tidal period) is the frictionless tidal wave–length in water with a constant depth H. In this particular case (see tabel 3) $L_{\mathrm{g}} \sim 450$ km. From this plot it can be seen that the equilibrium bed profile has a constant slope for small L/L_{g}. If L is increased the bed becomes deeper near the entrance of the embayment. This phenomenon was already explained in section 4. A maximum depth of about $21\,\mathrm{m}$ is reached near $L = 0.28L_{\mathrm{g}}$, which in this case corresponds to an embayment length of 135 km. For $L \gtrsim L_{\mathrm{max}}$, with $L_{\mathrm{max}} \sim 0.28L_{\mathrm{g}}(\sim 135$ km$)$, no equilibrium bed profile can be found anymore. The length for which the maximum depth is reached depends on the model parameters. In this case it equals L_{max}, but in general it may be smaller. The existence of a maximum embayment length means that if initially an embayment with length larger than L_{max} is chosen, deposition of sediment will occur near the landward side such that the length reduces to L_{max}. It can be shown that the maximum embayment length is related to the frictional length of the M_2 tide. This will be discussed in more detail in the next subsection.

In figures 5(a) and 5(c), the amplitude of the equilibrium horizontal tide (scaled by $\epsilon\sqrt{gH}$) is plotted as a function of the dimensionless position x and the length ratio L/L_{g}. Note that the M_2 tide becomes resonant for an embayment length $L \sim 0.2L_{\mathrm{g}}$, which is approximately 90 km in this case. Hence tidal resonance occurs for a length which is slightly shorter than a quarter of the tidal wave–length, due to the influence of bottom friction. Obviously this well-known phenomenon still occurs in embayments with erodible bottoms which are in morphodynamic equilibrium. However, the shift towards smaller lengths is less than for channels with constant fixed depths, because longer embayments with a sandy bottom have larger maximum water depths.

From figures 5(b) and 5(d), which show contour plots of the phases (in radians) of the M_2 and M_4 tide as a function of x and L/L_{g}, it is clear that the character of the tidal wave changes with increasing length. For a fixed $L \ll L_{\mathrm{g}}$, the phases are almost independent of the position x, hence a standing wave is observed in the embayment. However, for longer L the characteristics of a travelling wave are observed.

In figure 6 contour plots are shown of the different contributions to the net sediment transport, as defined in equation 11. Here we recall that the total flux is zero in morphodynamic equilibrium and that in the present case $\beta = 0$. From these plots it can be seen that diffusive contributions are only important in a thin boundary layer at the entrance of the embayment (see figure 6(a)) for $L/L_{\mathrm{g}} > 0.1$ and at the end of the embayment for $L/L_{\mathrm{g}} > 0.15$. For larger embayment lengths, it is seen from figures 6(a)–6(f) that the net advective flux due to the principal tidal components in the velocity field and in the concentration field is approximately zero (the terms $u^{\mathrm{s}}C^{\mathrm{s}}$ and $u^{\mathrm{c}}C^{\mathrm{c}}$ are almost equal and of opposite sign). Similarly the net advective fluxes related to the overtides and the residual components in the

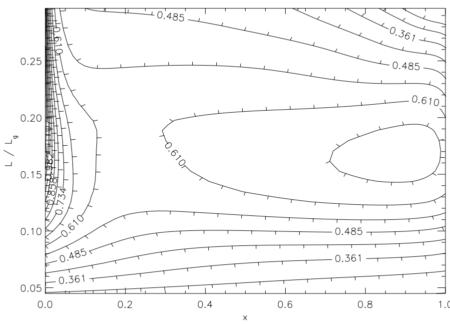

(a) Amplitude of the M_2 horizontal tide

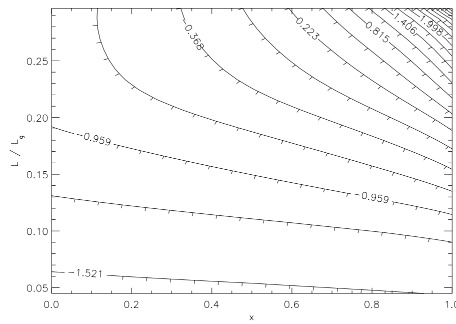

(b) Phase of the M_2 horizontal tide.

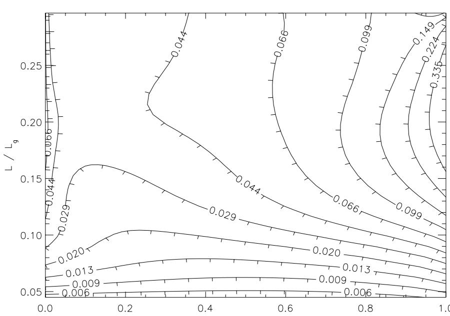

(c) Amplitude of the M_4 horizontal tide

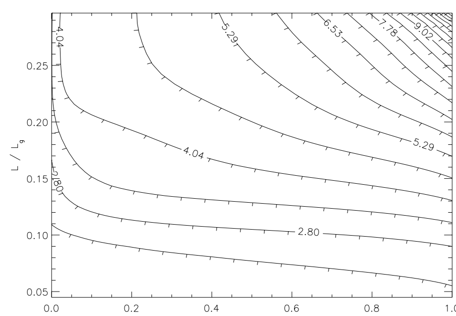

(d) Phase of the M_4 horizontal tide.

Figure 5: Contour plots of the amplitude and phase of the M_2 and M_4 horizontal tide in morphodynamic equilibrium as a function of the dimensionless coordinate x and the length scale ratio L/L_g. Velocities are scaled with $\epsilon\sqrt{gH}$, where ϵ is the nonlinearity parameter (see table 1). Parameters values are as in plate 4. The small ticks in the contour lines point to smaller contour levels.

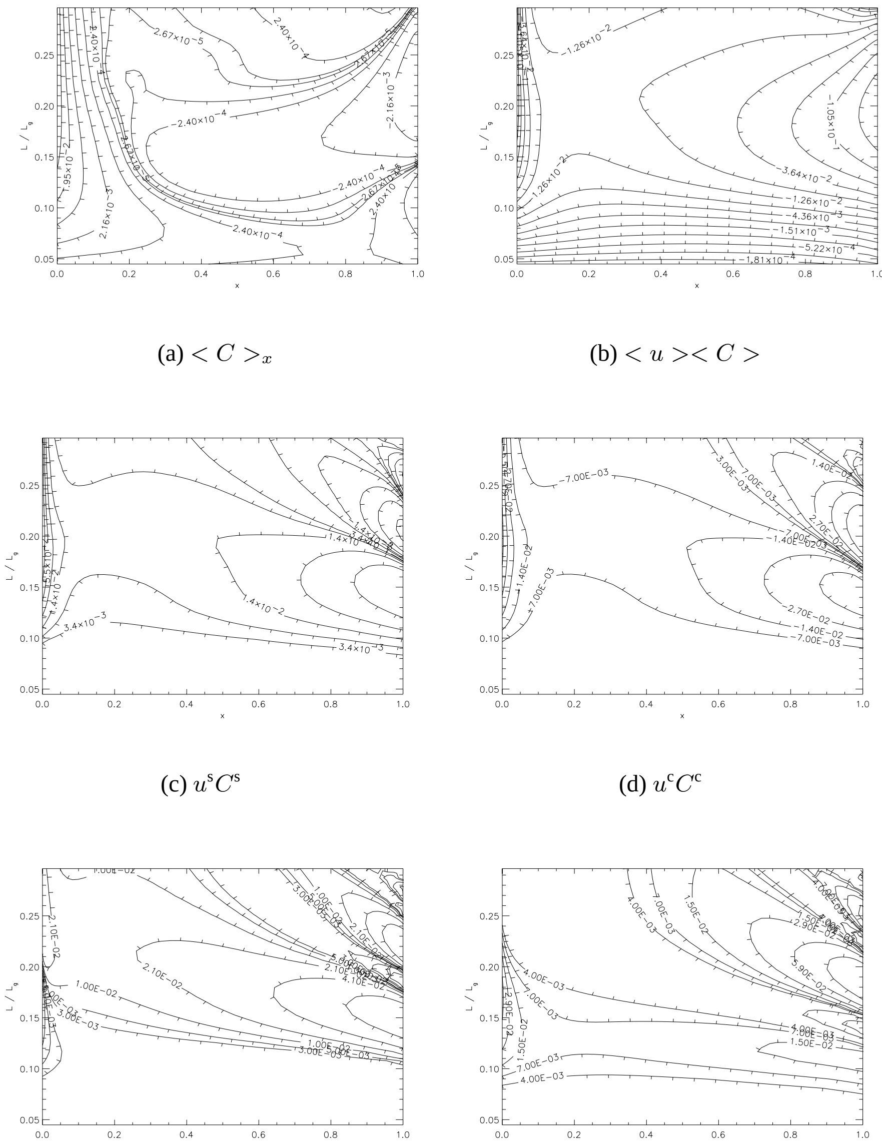

(a) $< C >_x$ (b) $< u >< C >$

(c) $u^{\mathrm{s}}C^{\mathrm{s}}$ (d) $u^{\mathrm{c}}C^{\mathrm{c}}$

(e) $u^{2\mathrm{s}}C^{2\mathrm{s}}$ (f) $u^{2\mathrm{c}}C^{2\mathrm{c}}$

Figure 6: Contour plots of the dominant contributions to the net sediment flux (defined in (11)) in morphodynamic equilibrium. Dependent variables are the dimensionless coordinate x and the length scale ratio L/L_{g}. The fluxes are scaled with $(\alpha/\gamma)\left(\epsilon\sqrt{gH}\right)^3$ (unit is kg $\mathrm{m}^{-1}\mathrm{s}^{-1}$ with α and γ the erosion and deposition constants defined in (2). Parameter values are as in plate 4.

velocity and concentration field vanish to a good approximation. For this type of morphodynamic equilibria the internal generation of phase differences between the velocity and concentration fields, caused by bottom friction, is essential. Therefore they will be referred to as friction-related morphodynamic equilibria.

5.2 Overtides, no phase difference

In the following numerical experiments an externally prescribed overtide was used with a phase difference $\phi = 0°$. The ratio of the M_4 amplitude and the M_2 amplitude at the seaward boundary, β, was varied between 0 and 0.15. Experiments were carried out for values of the other parameters as listed in table 3, which are representative for the Western Scheldt. Besides a case was studied in which the reference depth was increased to $H = 15$ m and the amplitude of the M_2 tide was decreased to $A = 1$ m. The latter choice, which was also used by De Jong (1998), results in a smaller friction coefficient r for a fixed embayment length. It turns out that $\beta = 0.074$ is a characteristic value for the Western Scheldt.

In figure 7 the dimensionless amplitude of the M_2 horizontal velocity (scaled by $\epsilon\sqrt{gH}$) at the entrance of the embayment is plotted as a function of embayment length and different values of β, *i.e.*, different strengths of the externally prescribed overtides. First of all it is noted that, even if an external overtide is prescribed, the resonance length of the embayment *in morphodynamic equilibrium* is slightly smaller than $0.25L_{\mathrm{g}}$. Furthermore it is seen that if the externally prescribed overtide is strong enough (see figure 7(a), $\beta = 0.15$ and figure 7(b), $\beta = 0.074$), embayment lengths can be found for which more than one morphodynamic equilibrium exists.

In general two different types of equilibria can be distinguished. As shown below this stems from the fact that both the externally prescribed M_2 tide and M_4 tide can show resonant behaviour. For embayment lengths smaller than a critical length L_{c} (e.g., in figure 7(a) $L_{\mathrm{c}} \sim 0.23L_{\mathrm{g}}$ for $\beta = 0.15$ and in figure 7(b) $L_{\mathrm{c}} \sim 0.28L_{\mathrm{g}}$ for $\beta = 0.074$) a new type of morphodynamic equilibria is found. One of the main differences with respect to the friction–related type of equilibria is that the water depths are now much larger. This can be seen from figures 8(a) and 8(c), which show contour plots of the bottom elevation h (defined in figure 2), scaled with the reference depth H, as a function of the dimensionless distance x to the entrance and the length ratio L/L_{g} for two different cases. These correspond to the default situation ($\beta = 0.074, \phi = 0$) and the situation with larger external overtides ($\beta = 0.15$). In figures 8(b) and 8(d) contour plots are shown of the phase of the M_2 tide as a function of x and L/L_{g} for the same two cases. They show that the new equilibrium is characterized by a standing tidal wave: for a fixed $L < L_{\mathrm{c}}$ the phase is almost spatially uniform. Furthermore, it appears that the vari-

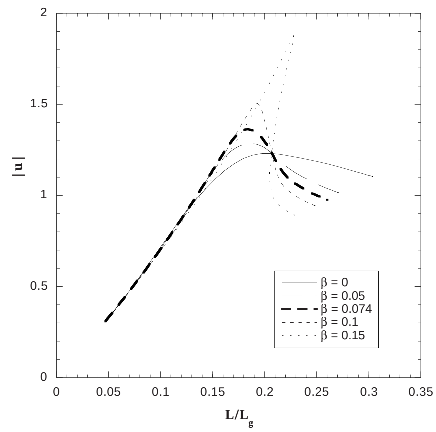

(a)

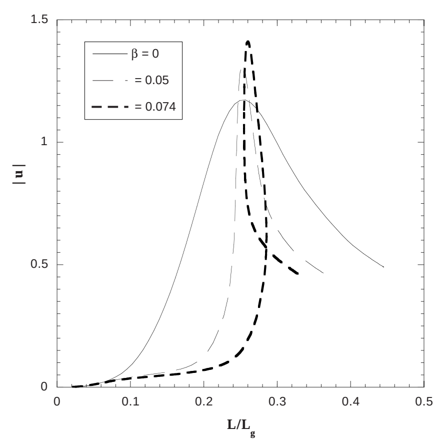

(b)

Figure 7: Dependence of the amplitude of the M_2 horizontal velocity at the entrance of the embayment on the dimensionless length L/L_g for different values of β. The velocity is scaled with $\epsilon\sqrt{gH}$. In a. the parameter values specified in table 3 are used; in b. the reference water depth $H = 15$ m and the amplitude of the M_2 tide at the entrance is $A = 1$ m.

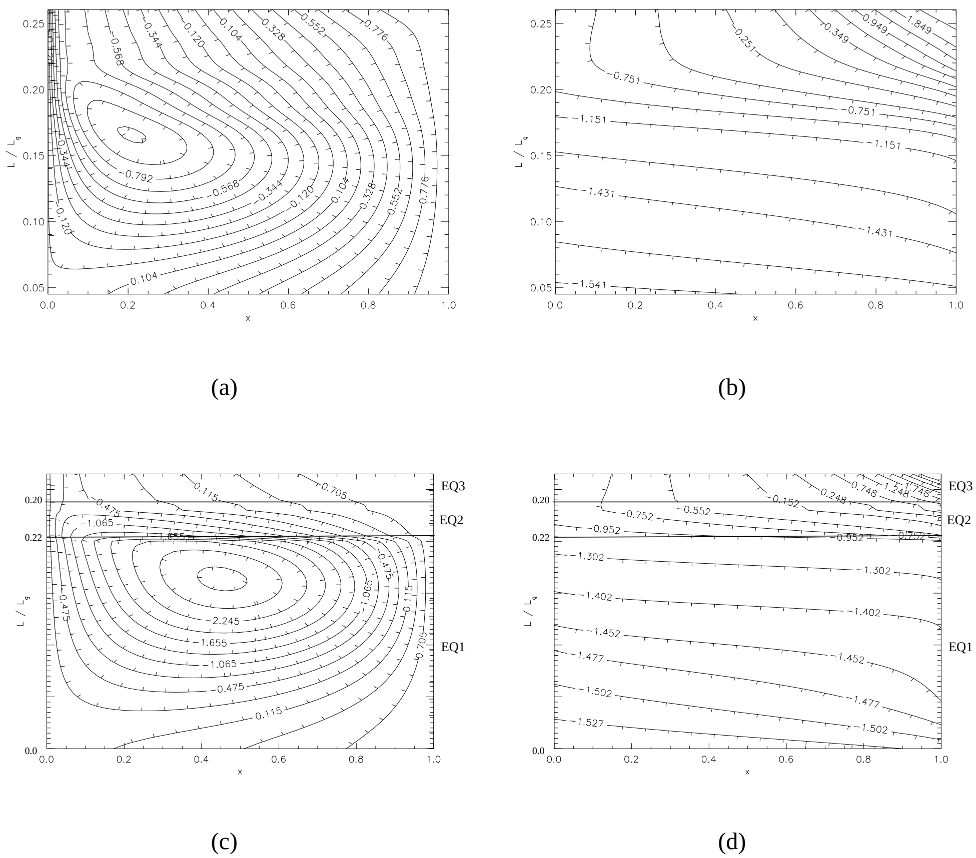

Figure 8: Contour plots of the equilibrium bed profile h (scaled with reference depth H) and of the phase of the M_2 vertical tide. Dependent variables are the dimensionless coordinate x and the length scale ratio $L/L_{\rm g}$. In a. and b. the parameter values of table 3 are used (compare with figure 7(a)) and in c. and d. $H = 15$ m and $A = 1$ m (compare with figure 7(b)).

ous contributions to the total net sediment flux, as defined in (11), have completely different magnitudes. It turns out that the main contributions are now due to the advective terms $u^{\rm s}C^{\rm s}, u^{\rm s}\hat{C}^{\rm s}, u^{2\rm c}C^{2\rm c}$ and $\hat{u}^{2\rm c}C^{2\rm c}$. Contour plots of contributions (as a function of x and L/L_g) are shown in plate 9 for the same parameter values as used in figures 8(c) and 8(d). Results for other parameter values yield qualitatively similar results as long as $L < L_{\rm c}$. Now an approximate balance can be observed between $u^{\rm s}C^{\rm s}$ and $u^{\rm s}\hat{C}^{\rm s}$, as well as between $u^{2\rm c}C^{2\rm c}$ and $\hat{u}^{2\rm c}C^{2\rm c}$. Hence, net advec-

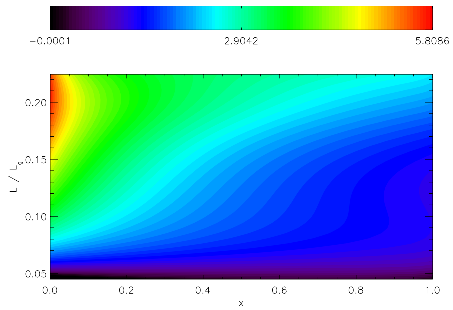

(a) $u^{\mathrm{s}}C^{\mathrm{s}}$

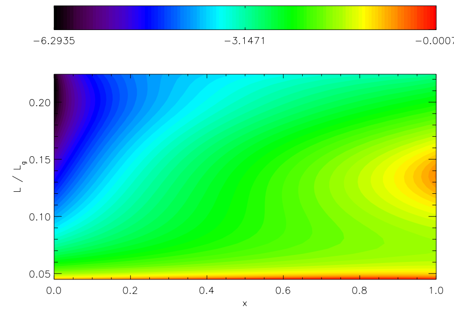

(b) $u^{\mathrm{s}}\hat{C}^{\mathrm{s}}$

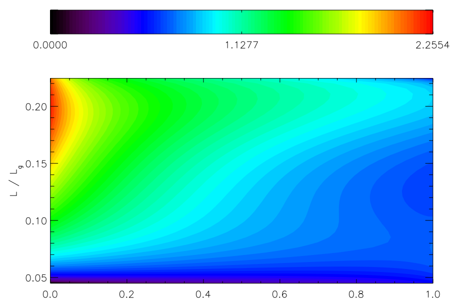

(c) $u^{2\mathrm{c}}C^{2\mathrm{c}}$

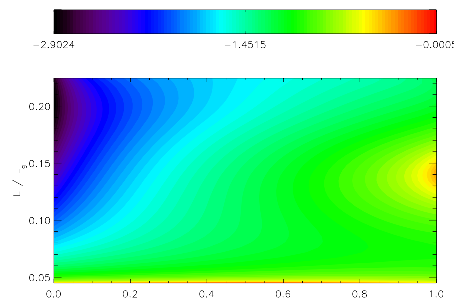

(d) $\hat{u}^{2\mathrm{c}}C^{2\mathrm{c}}$

Figure 9: Contour plots of the dominant contributions to the net sediment flux (defined in (11)) for the morphodynamic equilibrium which owes its existence to the presence of external overtides. Dependent variables are the dimensionless coordinate x and the length scale ratio L/L_{g}. The scaling for the fluxes is identical to that in figure 6. Here $\beta = 0.15$, other parameter values are as in table 3.

tive fluxes which are solely due to *internal nonlinear* interactions are compensated by net advective fluxes which are induced by external overtides.

Since the external overtides are important to maintain this morphodynamic equilibrium, it is to be expected that the critical length L_{c}, beyond which this equilibrium ceases to exist, is related to the resonance length of the M_4 tide. This is because for $L > L_{\mathrm{c}}$ the amplitudes of the external M_4 horizontal and vertical tide rapidly decrease. Indeed, this supposition is confirmed by the model results: L_{c}

turns out to be slightly larger than the M_4 resonance length, multiplied by the factor β/ϵ. The latter accounts for the fact that sediment fluxes related to external overtides have to be of the same order as those generated by internally generated overtides to maintain the equilibrium.

For embayment lengths $L > L_\mathrm{c}$ morphodynamic equilibria can still exist, but internally generated M_4 tides are much more important. In this case the main contributions to the net sediment flux come from the terms in (11) which are related to pure M_2–forcing. The results are similar to the results already shown in figure 6. Furthermore, the water motion in this equilibrium is characterized by a travelling tidal wave, as can be seen from figure 8. This implies that bottom friction plays an important role, hence this equilibrium is the *frictional–related* equilibrium which also exists if $\beta = 0$, see the previous subsection.

It appears that in case external overtides are present, the friction–related morphodynamic equilibrium can no longer exist for lengths $L < L_\mathrm{s}$. If external overtides are small ($\beta \ll \epsilon$) then $L_\mathrm{s} = L_\mathrm{c}$ and there is a smooth transition from the morphodynamic equilibrium controlled by external overtides to the friction–related equilibrium. However, a more general expression for L_s is $L_\mathrm{s} = \min(L_\mathrm{c}, L_{M2})$, where L_{M2} is slightly smaller than the resonance length of the principal tide. The latter is defined as the length for which the amplitude of the horizontal M_2 tide at the entrance attains a maximum. As can be seen from figures 8(b) and 8(d) it also marks the transition where the principal tide changes its character from a standing wave to a travelling wave.

Now an interesting situation occurs if external overtides are sufficiently strong ($\beta \geq \epsilon$) such that the maximum length L_c of the equilibrium related to external overtides exceeds the minimum length L_s of the friction–related equilibrium. In that case there is a range of embayment lengths (between L_s and L_c) for which multiple morphodynamic equilibria exist which have completely different characteristics. As shown in figure 8 in this range of embayment lengths there is a third (unstable) equilibrium which connects the two previously mentioned equilibria in a smooth way.

In the appendix it is demonstrated, by using a simple model, that morphodynamic equilibria can only exist as long as the embayment length is shorter than the frictional length scale L_f of the M_2 tide. An expression for L_f is given in 17. Note that L_f depends on the actual length L and also on implicitly on parameter β through the parameter H_max. Here H_max is the maximum water depth corresponding to a given morphodynamic equilibrium. Now the maximum embayment length is determined by the condition $L_\mathrm{max} = L_\mathrm{f}(L_\mathrm{max})$. Predictions of this simple model are in good agreement with the results of the full model. It appears that L_max decreases with increasing values of β (see figure 7) due to the fact that the maximum water depths corresponding to the friction–related equilibrium become smaller in this case.

6 Comparison with Field Observations

We now briefly discuss the validity of the model by comparing its results with data of the water motion, suspended sediment concentration and bathymetry of some tidal embayments.

According to our model, if the length of the embayment is much shorter than the tidal wave–length, morphodynamic equilibria are characterized by a spatially uniform horizontal and vertical tide. The corresponding *depth–integrated* concentration is constant which implies that the depth–averaged concentration increases towards the landside of the embayment. Furthermore, the bottom profiles have an almost constant slope.

Field observations at various positions in the Frisian Inlet, as discussed in Van de Kreeke & Dunsbergen (to appear); Wang *et al.* (1995), indeed indicate that to a first approximation the vertical tide has a constant amplitude in this embayment. The prediction of a spatially uniform tidal current amplitude is consistent with the field data discussed by Friedrichs (1995), from which it appears that in equilibrium the bed shear stress is uniform. The latter result is closely related to the empirical relationship between tidal prism P and the cross–sectional area A, which was discussed by O'Brien (1969) and reads $P = cA$. This relation is also satisfied by our simple model and yields for the constant $c = \pi U/\sigma$. In case of the Frisian Inlet system (see table 2) $c \sim 0.67\mathrm{m\,s^{-1}}$ which agrees well with the empirically obtained result of O'Brien (1969), see also De Vriend (1996). Note that the constant c, according to our model, is not related to the critical erosion velocity of the sediment.

The observed increase in the concentration towards the land is consistent with the observations discussed by Postma (1954). In our model this property stems from a diffusive flux which is proportional to the depth–integrated rather than the depth–averaged concentration. This parameterization accounts for a net landward sediment flux induced by waves. Unfortunately, detailed measurements on spatial distributions of cross–sectionally averaged sediment concentrations in embayments are scarce.

A comparison between the equilibrium bottom profiles, predicted by a one–dimensional model and observed profiles in seven different short embayments located in the Dutch Wadden Sea was carried out by De Swart & Blaas (1998). They concluded that all these systems are characterized by monotonically decreasing water depths towards the land and that this decrease is almost uniform. Small deviations from the constant slope profile can be attributed to the influence of the finite embayment length (as shown in this paper), bottom friction and external overtides.

Finally we have compared the results of our model with field data gathered in the Western Scheldt estuary (see figure 1). The data were provided by the National Institute of Coastal Management/RIKZ in Middelburg and consists of sea surface elevations and bathymetric information at various locations in the estuary. Available data on the current velocities and concentrations appeared to be restricted to a number of relatively short timeseries at isolated positions. Since our model yields information about cross-sectionally averaged quantities, these data could not be used.

In figures 10(a) and 10(c) the amplitudes of the M_2 and M_4 tidal constituents of the sealevel variations are shown as functions of the distance to the seaward boundary of the Western Scheldt. Similarly the corresponding phases of the M_2 and M_4 constituents are shown in figures 10(b) and 10(d). The data are indicated by the circles and are extracted from the observed timeseries of the sea surface variations by application of Fourier analysis. The solid curves represent model results. The one with $s = 0$ has been obtained with the basic model for a rectangular basin, as discussed in this paper. The other curve (with $s = -4$) shows the results obtained with a modified version of our model, which allows for an exponential width convergence of the embayment (length scale $L_b = L/|s|$). The formulation of this model has been adopted from Friedrichs & Aubrey (1994). As can be seen in figure 11(a) the value $s = -4$ is a best fit for the Western Scheldt, but this yields a slight overestimation of the width convergence in the marine part.

As can be seen, there is fairly good agreeement between the model results and the observations, considering the many simplifying assumptions underlying the present model. Noticeable discrepancies occur at distances larger than $0.8L$, which is in the river part of the estuary. However, this part cannot be captured well by the present model, because river effects are neglected. This was done because the main interest is in the morphodynamic behaviour of the marine part, where the river influence is small. Another discrepancy is the underestimation by the model of the resonance peak of the M_2 tide near Antwerp, although the location agrees remarkably well with the observed resonance position. The underprediction is partly due to the neglect of the width convergence of the estuary.

Finally, in figure 11(b) the predicted equilibrium bathymetry for the Western Scheldt is compared with field data. For the selected values there is only one morphodynamic equilibrium in the model. The general trends are rather well predicted, although some discrepancies can be observed as well.

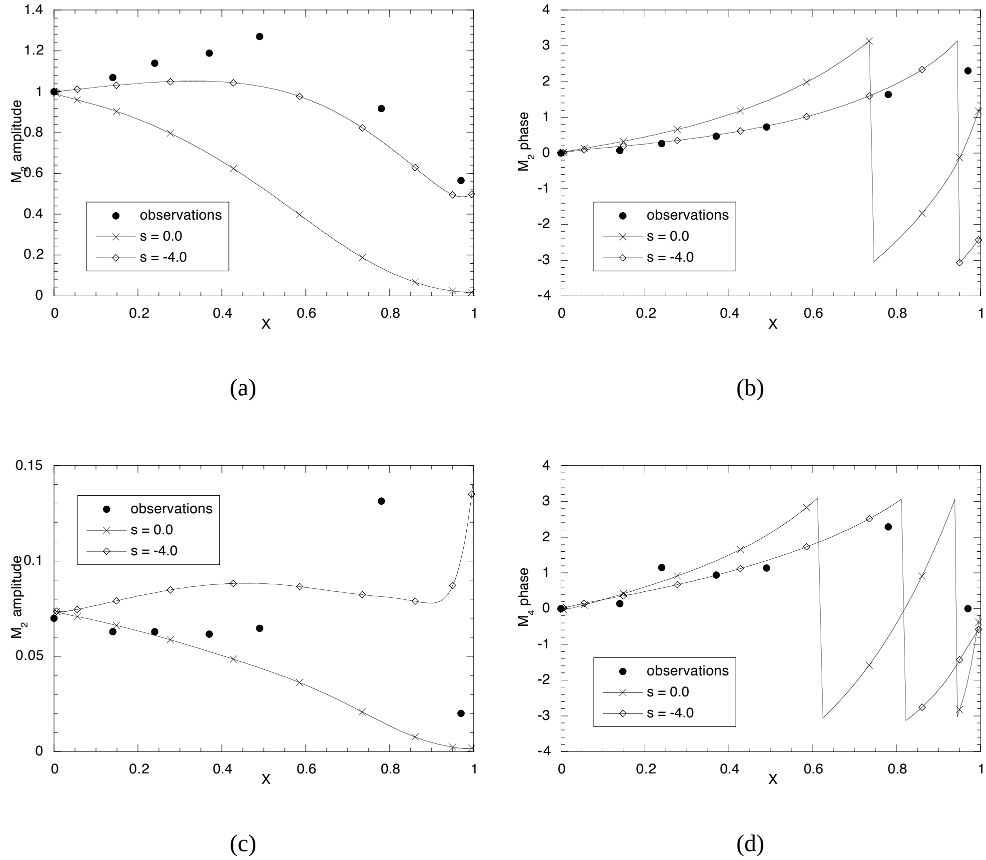

Figure 10: Comparison of field observations and model results for the water motion in the Western Scheldt estuary. Shown are the width-averaged amplitudes and phases of the M_2 and M_4 tidal constituents in the water level versus the distance to the seaward boundary. The basic model result is denoted by the solid curve with $s = 0$. The curve with $s = -4$ has been obtained with a modified version of our model in which the exponential width convergence of the estuary (length scale $L_\mathrm{b} = -L/s$) is incorporated; for further details see the text.

7 Time Evolution of One–Dimensional Bed Profiles

For some values of the parameters three equilibria were found, two of them are stable and one is unstable with respect to small perturbations. To gain some insight in the global characteristics of these equilibria, it is important to study the time evolution of large perturbations.

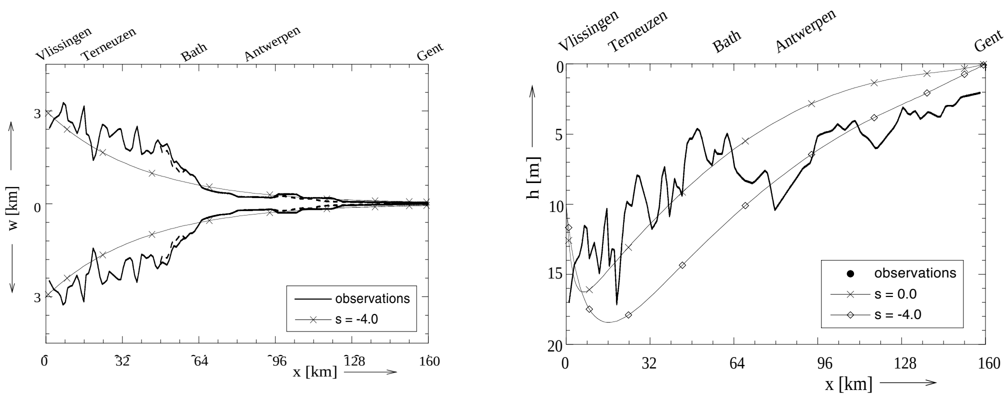

(a) Width of the Western Scheldt estuary .

(b) Width averaged depth of the Western Scheldt estuary .

Figure 11: Comparison of observation and model results for the width and width–averaged depth of the Western Scheldt.

The parameter values used are given in table 3. With an embayment length of $L = 150\,\mathrm{km}$ two stable equilibria were found, one which was relatively deep (approximately $100\,\mathrm{m}$) while the other one was relatively shallow (maximum depth of about $30\,\mathrm{m}$). In figure 12 an example of the time evolution of a finite perturbation on the shallow equilibrium is shown. One observes that first the system starts to rearrange the sediment in the estuary and to import sediment from the sea. Next, the system returns slowly to its equilibrium state. In this experiment the bed evolution is calculated for about 4500 years. Hence the adaptation to equilibrium takes place at a long time–scale. This and other experiments show that the equilibria have an ”order–one” region of attraction and hence cannot be easily forced from the ”shallow” one to the ”deep” situation.

8 Two–Dimensional Perturbations

It is not clear at all if the one–dimensional equilibria are stable with respect to (small) perturbations. In this section, we will focus on the stability properties of the basic state with respect to both one and two dimensional perturbations.

Consider perturbations which evolve on the equilibrium as discussed in sec-

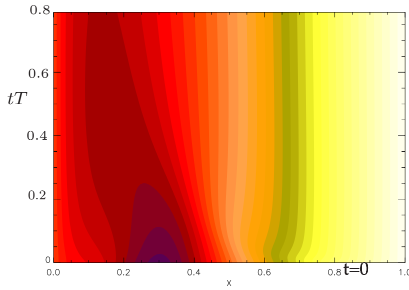

(a) Time–position in basin diagrams of the bed

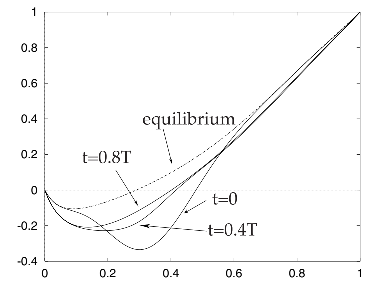

(b) Bed profiles at $t = 0$, $t = 0.4T$ and $t = 0.8T$ and the equilibrium bed profile. $t = 5500$ year.

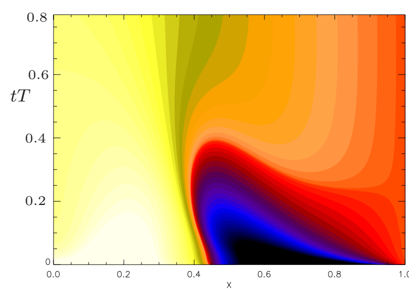

(c) Time–position in basin diagrams of the flux

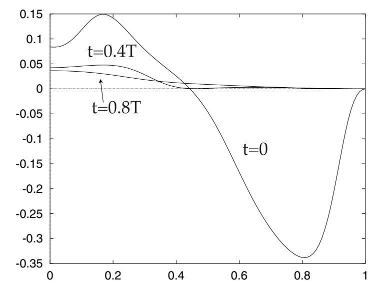

(d) Flux profiles at $t = 0$, $t = 0.4T$ and $t = 0.8T$. $T = 5500$ year.

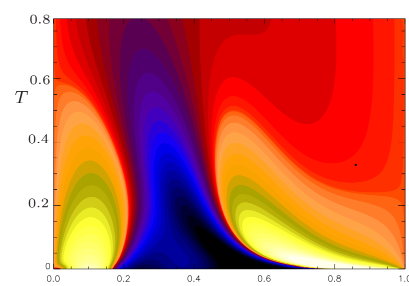

(e) Time–position in basin diagrams of the divergence of the flux.

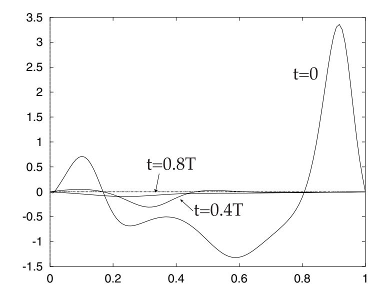

(f) Profiles of the divergence of the flux at $t = 0$, $t = 0.4T$ and $t = 0.8T$. $T = 5500$ year.

Figure 12: Time evolution of an embayment with $L = 150$ km. The system is forced with both an M_2 and a M_4 tide.

tion 5. In the equations of motion the following expressions are substituted:

$$\Phi = \Phi_{\text{eq}} + \Phi' \tag{13}$$

where $\Phi = (\zeta, u, v, C, h)^T$ is the solution vector and Φ_{eq} as given in section 5. In (13), the superscript $'$ labels the perturbations which are considered to be small with respect to the basic variables. Next, the equations (5) are linearized with respect to these perturbations. The linearized bed evolution equation reads

$$h'_\tau - \frac{x}{L_{\text{eq}}} L'_\tau h_{\text{eq},x} = -\left\langle 2.0 u_{\text{eq}} u' - C' \right\rangle + \lambda \left[\left(|\vec{u_{\text{eq}}}|^b h'_x \right)_x + \left(|\vec{u_{\text{eq}}}|^b h'_y \right)_y \right] \tag{14}$$

Careful inspection of the linearized equations shows that the lateral structure of the perturbations reads:

$$(u, \zeta, C, h, L)' = \sum_{n=0}^{\infty} (u, \zeta, C, h, L)_n \cos(l_n y) \tag{15a}$$

$$v' = \sum_{n=0}^{\infty} v_n \sin(l_n y) \tag{15b}$$

The stability of a short ($L = 20$km), an intermediate ($L = 50$km) and long ($L = 160$km) embayment is studied.

The diffusive limit for a short embayment has been extensively studied in Schuttelaars & De Swart (1999). In this limit it is assumed that the main contribution to the net sediment transport is due to diffusion. It was found that the bed could become linearly unstable. A necessary condition for instability is the presence of frictional bottom torques by which the tidal velocity decreases over shoals and increases in the channels. If the effect of frictional torques is stronger than the continuity effect (which causes water to slow down in channels and increase over shoals), the bed perturbations start to grow.

However, the order of magnitude of the ratio of advective and diffusive divergences of sediment is given by μ/ϵ^2 which is $\mathcal{O}(1)$ in this case. Hence even for an embayment length of $20\,$km the advective and diffusive fluxes might be of the same order. In figure 13 the largest eigenvalue is plotted as a function of the parameter $l_{\text{n}} n\pi L/B$. Here n gives the number of zeros in the lateral direction and B is the width of the embayment. First of all, it is observed that the maximum growth rate is reached for much larger l_{n} values, compared with Schuttelaars & De Swart (1999). However, one should be careful making this comparison since both the friction and the bed–slope parameter λ are different. Here $\lambda \sim 10^{-7}$

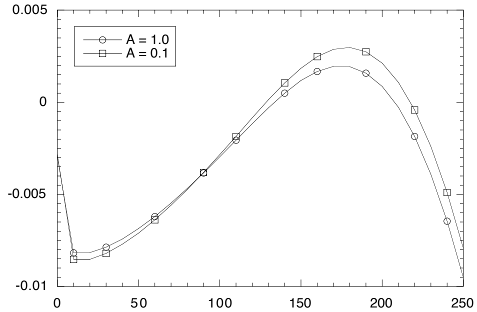

Figure 13: Growth rates of the most unstable mode for an estuary of $L = 20\,\mathrm{km}$.

whereas in Schuttelaars & De Swart (1999) $\lambda \sim 10^{-6}$. For the latter value of λ the system becomes only unstable for $r \sim 0.125$. Hence the stabilizing effect of gravity is stronger than the destabilizing effect of sediment diffusion. The same is observed here: define the points l_{l} and l_{r} as the first and second value of l_{n} at which the mode becomes neutral (*i.e.* where the growth rates are 0). Left of l_{l} and right of l_{r} the diffusive mechanism is still destabilizing. However, the effect of the bed–slope term stabilizes the eigenmode. For $l_{\mathrm{n}} \ll l_{\mathrm{l}}$ the diffusive mechanism is stabilizing: high concentrations are found over the shoals. For $l_{\mathrm{n}} \sim 150$ the diffusive mechanism has a positive feedback with the bed: a higher concentration is observed in the channels and hence sediment is transported from the channels towards the shoals (see figure 14).

To study the influence of advection on the eigenvalue, the Strouhall number $\epsilon = A/H$, which measures the strength of the nonlinearities is reduced by reducing the amplitude of vertical tide by a factor 10, keeping the friction parameter r constant by increasing the drag coefficient with the same factor. For $l_{\mathrm{n}} \ll 1$ the divergence of the advective fluxes is stabilizing since in this regime its contribution can be rewritten as a diffusive term with positive diffusion coefficient (see Schuttelaars (1997)). If l_{n} is increased, it becomes destabilizing while for very large values the advective contribution is stabilizing again. This can be understood as follows: in leading order the time–independent concentration reads

$$< C >' = u^{\mathrm{s}} u^{\mathrm{s}'} + a\epsilon \left(u^{\mathrm{s}} C^{\mathrm{s}'} \right)_x$$

with $C^{\mathrm{s}'} \simeq u^{\mathrm{s}} u^{0'}$. In the case of a short embayment this can be shown explicitly comparing the order of magnitudes of the different terms. Using this approximation and the fact that $u^{\mathrm{s}} \simeq -1$, the leading order bed evolution equation reads

$$h'_\tau = a\mu \nabla^2 \left(-u^{\mathrm{s}'} + a\epsilon u^{0'}_x \right) - a\epsilon u^{0'}_x$$

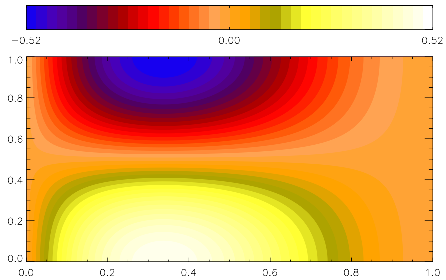

(a) Bed eigenfunction for $n = 1$ and $l_1 = 30$.

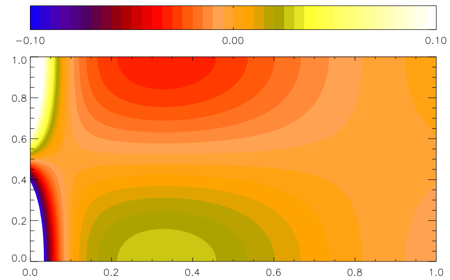

(b) Concentration eigenfunction for $n = 1$ and $l_1 = 30$.

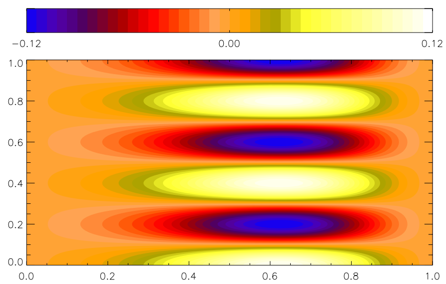

(c) Bed eigenfunction for $n = 5$ and $l_5 = 150$.

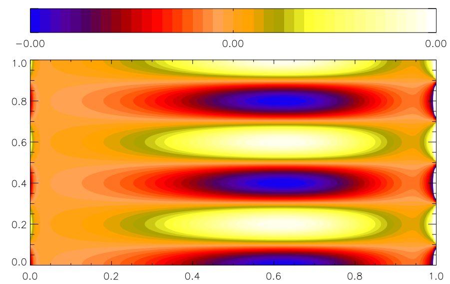

(d) Concentration eigenfunction for $n = 5$ and $l_5 = 150$.

Figure 14: Contour plots of bed and concentration profiles for both a stable and unstable mode.

For the perturbations under study, the second term in the diffusive contribution (which is due to advection) results in a higher concentration over the shoals than over the troughs. Hence this term is always stabilizing. The advective term is always destabilizing: sediment is transported away from the troughs and up the crests. Comparing the ration of the advective diffusion and advection, which is given by $a\mu l_{\mathrm{n}}^2$, it is clear that the advective contribution is destabilizing for $a\mu l_{\mathrm{n}}^2 < 1$ and stabilizing for $a\mu l_{\mathrm{n}}^2 > 1$. Because the effectiveness of the stabilizing effect depends on the effectiveness of the diffusive mechanism, the two regimes are shifted towards smaller values of l_{n}.

By reducing the diffusion coefficient from $\mu^\star = 100\mathrm{m}^2\mathrm{s}^{-1}$ to $\mu^\star = 1\mathrm{m}^2\mathrm{s}^{-1}$ the effects of advection can be studied in more detail. To simplify this analysis, the amplitude of the external overtide β is put to 0. Again the effect of the advective term is studied by changing the amplitude of the external forcing from $A = 1$ m to $A = 10$ cm while keeping the friction parameter constant. Now the system is only unstable if advection is strong enough compared to the bed slope contribution. If $A = 10$ cm no instabilities are found (see figure 15); the eigenmodes resemble the eigenmodes found in limit with neither advective nor diffusive convergences of suspended sediment (hence they are solutions of the eigenvalue problem $h_\tau \simeq \lambda\nabla^2 h$). If $A = 1$ m, instabilities are found. However, they differ considerably from the

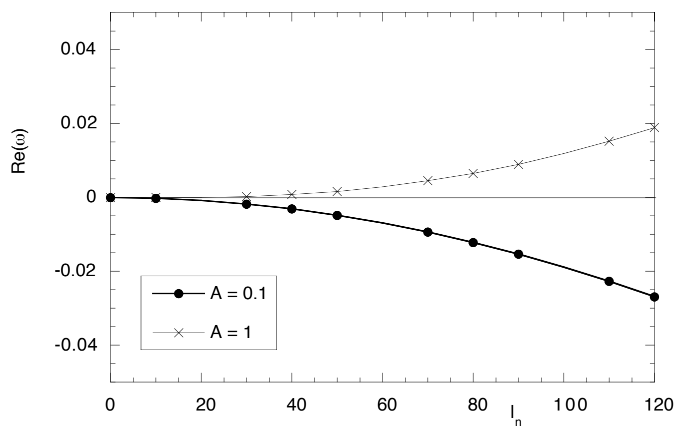

Figure 15: Growth rates of the most unstable mode for an estuary of $L = 20$ km for different amplitudes A.

diffusive ones. Careful comparison of the magnitudes of the divergences of the diffusive and advective sediment fluxes shows that they are still of the same order due to large gradients in the concentrations (even though $\mu/\epsilon^2 \ll 1$ $l_\mathrm{n}^2\mu/\epsilon^2$ can still be of order one). By taking the advective limit ($\mu = 0$ and allowing for a net sediment flux at the landside of the embayment) one can show that only for $\mu \ll 1.0$ the diffusive contributions to the convergence of the net sediment flux can be neglected. Therefore, only two types of modes can be found for realistic values of μ: diffusive modes and mixed modes. No purely advective modes will be found. The diffusive modes become unstable due to the mechanism as described in Schuttelaars & De Swart (1999), while the mixed modes become unstable because of the destabilizing effect of advection. The longitudinal structure of the eigenmodes becomes much more complicated when μ is decreased. In figure 16 the bottom eigenmodes for different external forcings are shown.

The limit for large l_n as derived in Schuttelaars & De Swart (1999) is still valid.

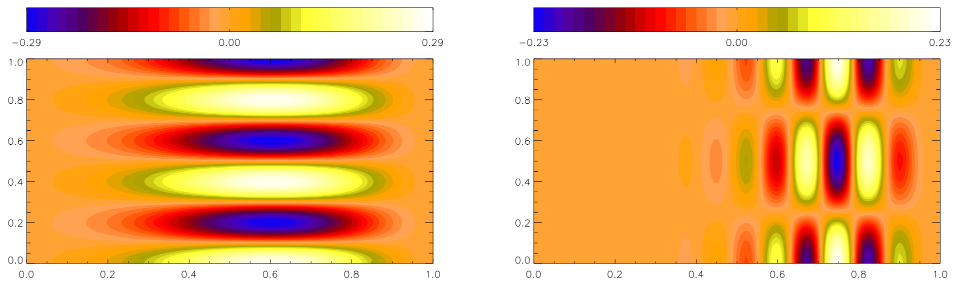

(a) Bed eigenfunction for $A = 0.1$.

(b) Bed eigenfunction for $A = 1.0$.

Figure 16: Contour plots of bed profiles for different values of A.

The system becomes stable for large values of l_n only because of the stabilizing effect of the bedslope term.

The contributions to the divergence of the sediment flux consists of three different parts: a direct contribution to the time–independent concentration which is of order β^2, an indirect contribution to the time–independent concentration due to the advective terms (order $\beta\epsilon$) and a direct advective contribution (order $\beta\epsilon$).

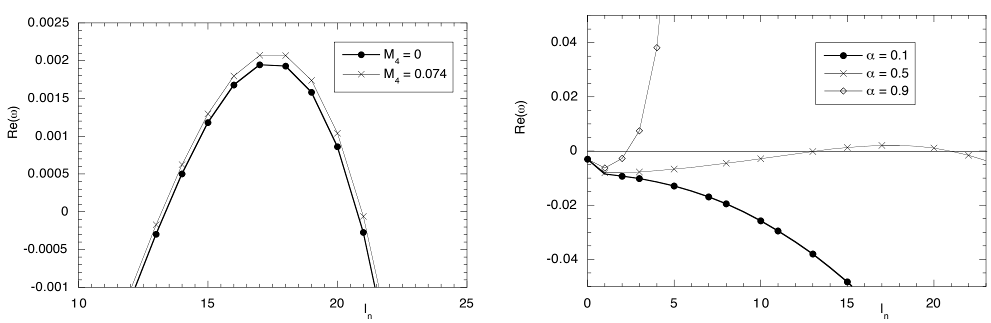

(a) Comparison of eigenvalues of the most unstable modes for different M_4 forcings.

(b) Comparison of eigenvalues of the most unstable modes for different values of α.

Figure 17: Most unstable eigenmodes.

Figure 17(a) suggests that for $L = 20\,\text{km}$ and all values of l_n the overtides are destabilizing. Which of the aforementioned contributions is responsible for this is still under study.

The stability of the equilibrium for small perturbations id very sensitive to the dependence of the bottom friction parameterization on the local water depth. This sensitivity is studied by varying the coefficient α. It is to be expected that for larger values of α the system becomes more unstable since stronger frictional torques can be generated (see figure 17(b)). Furthermore the perturbations will concentrate at the end of the embayment where the bottom friction is most efficient (see figure 18).

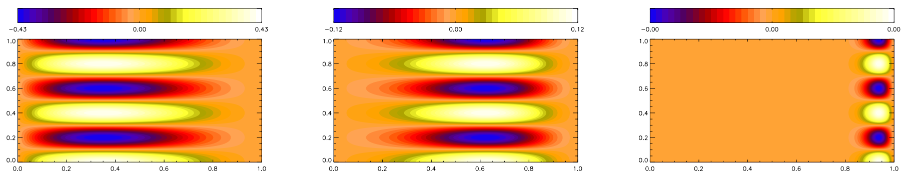

(a) Bed eigenfunction for $\alpha = 0.1$.

(b) Bed eigenfunction for $\alpha = 0.5$.

(c) Bed eigenfunction for $\alpha = 0.9$.

Figure 18: Comparison of the bed profile for $n = 5$ and $l_5 = 150$ for different values of α.

In the next experiments the length of the embayment is increased to $L = 50\,\mathrm{km}$ and the drag coefficient reduced to $C_{\mathrm{D}} = 0.0008$. The two different possible instabilities are easily observed: the most unstable eigenmode for relatively small l_{n} is a mixed mode. For $l_{\mathrm{n}} \sim 260$ the second mode becomes more unstable (see figure 19) than the mixed mode. The second mode turns out to be a purely diffusive mode. In figure 20 the first two eigenmodes of the bed are plotted. It is observed that the first eigenmode has a completely different structure than any of the diffusive ones: it is concentrated near the entrance. Furthermore the advective and diffusive fluxes are of the same order. The second eigenmode is a real diffusive one. Of course, by decreasing the diffusion coefficient $\mu^{\star}$ the advective properties of the eigenmodes become clearer.

For an embayment with a length of $50\,\mathrm{km}$ the overtides are stabilizing. This means that for this embayment length the stabilizing contributions due to externally prescribed overtides exceed the destabilizing ones (see figure 21(a)). Another interesting feature is that both diffusive and mixed can become unstable simultaneously (see figure 21(a), $M_4 = 0.035$). The (de)stabilizing influence of advection is still similar to the case with $L = 20\,\mathrm{km}$. Now for $l_{\mathrm{n}} < 40$ advection is stabilizing, while for larger l_{n} the advective contributions are destabilizing.

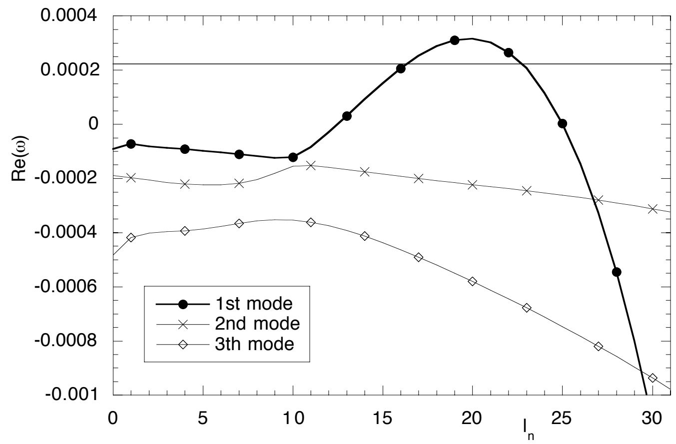

Figure 19: Growth rates of the three most unstable modes for an estuary of $L = 50\,\mathrm{km}$.

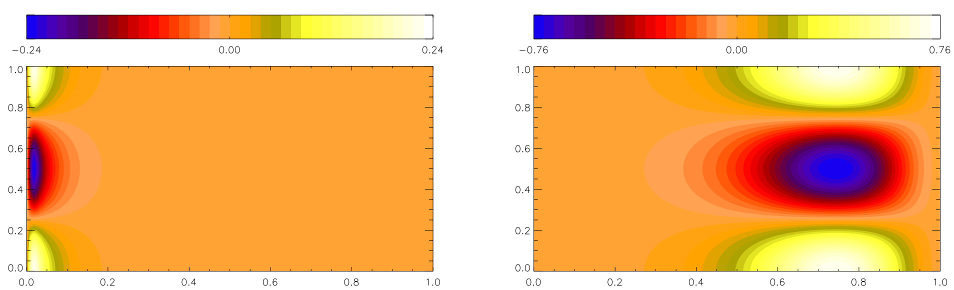

(a) First bed eigenfunction.

(b) Second bed eigenfunction.

Figure 20: Contour plots of the two most unstable bed profiles for for $n = 2$ and $l_1 = 200$.

For very long estuaries ($L = 160\,\mathrm{km}$) comparable behaviour is found. The drag coefficient has been reduced to $C_\mathrm{D} = 0.0001$. Since μ scales with the embayment length L^{-2} the diffusive contributions are much smaller and hence most eigenmodes have a mixed modes character.

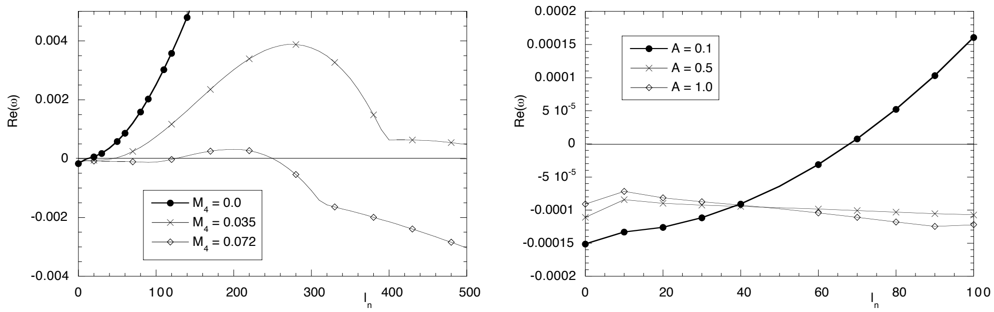

(a) Comparison of eigenvalues of the most unstable modes for different M_4 forcings.

(b) Comparison of eigenvalues of the most unstable modes for different values of α.

Figure 21: Comparison for $n = 0$ of the first eigenmode for fixed and variable embayment length.

9 Conclusions

In this contribution an idealized one–dimensional model has been analyzed to gain more understanding of the morphodynamics in long embayments. If the embayment length is much smaller than the tidal wavelength, the momentum equation describes in leading order a pumping mode, if the length is increased, both resonance effects and bottom friction become more important.

Sediment is transported as suspended load, both due to diffusive and advective processes. For a short embayment, the diffusive transport mechanism is most important. However, if the channel length is increased, diffusion becomes less effective and advection is the main transport mechanism. The latter is due to both external and internally generated overtides.

On of the aims was to investigate the possible existence of equilibria. A system is said to be in morphodynamic equilibrium when the averaged sediment flux vanishes throughout the embayment. The water motions in the embayment are forced by externally prescribed M_2 and M_4–tides. Furthermore overtides were generated internally. Using the knowledge of the short embayment limit and numerical continuation techniques, it was shown that equilibrium profiles exist for embayment lengths smaller than the M_2 frictional length. Embayments longer than M_2 frictional length tend to fill up until the maximum embayment length is reached. It was observed that the embayment became resonant for a length of approximately 0.25 times the gravitational wave length. It is well known that the resonance length L_{res} of a frictionless embayment with a flat bottom is 0.25 times the gravitational wave length. An important finding here is that this value is maintained even in a frictional domain due to adjustments of the bottom. Furthermore, it was shown that character of the tidal wave changed from a standing wave character towards a running wave.

If the amplitude of the externally prescribed M_4–tide is large enough compared to the amplitude of the M_2–tide, multiple equilibria can be found. This means that for the same parameter values more than one morphodynamic equilibrium bed profile exists. These bed profiles have totally different characteristics and may have large practical consequences. For example large interferences in an estuary with multiple equilibria may lead to sudden geometrical changes and different tidal characteristics.

A Frictional Length Scale

In this appendix, the frictional length scale for the M_2 tide of an embayment is studied. Following Friedrichs & Madsen (1992), to calculate the frictional length scale, a spatially uniform water depth is chosen. Since this water depth has to be representative for the equilibrium, the maximum water depth H_{max} is chosen in the continuity equation. Since the choice of the maximum water depth underestimates the frictional strength at the end of the embayment considerably, a frictional depth H_{f} is defined as follows:

$$\frac{1}{H_{\mathrm{f}}} = \int_0^1 \frac{dx}{1-h}$$

The dimensionless equations now become:

$$\zeta_t + \left[\frac{H_{\mathrm{max}}}{H} u\right]_x = 0 \tag{16a}$$

$$u_t + \lambda^{-2}\zeta_x + \frac{ru}{\mu H_{\mathrm{f}}} = 0 \tag{16b}$$

with μ a constant between 0 and 1.

These equations have solutions of the type

$$(u,\zeta) = \Re\{(\hat{u}(x), \hat{\zeta}(x)\exp(i(kx-t))\}$$

where $\Re$ denotes the real part. This describes an incoming and reflected tidal wave with exponentially decaying amplitudes. Substitution of these expressions in (16) yields a solution for the complex wavenumber k. The dimensionless frictional length scale is $1/\Im(k)$ where $\Im$ denotes the imaginary part. After using the definition of parameter r (see table 1) the dimensional frictional length scale becomes

$$L_{\mathrm{f}} = \frac{2\pi\sqrt{gH_{\max}}}{\sigma}\left[\frac{2}{-1+\sqrt{1+\left(\frac{8C_{\mathrm{D}}AL}{3\pi\mu H_{\mathrm{f}}H}\right)^2}}\right]^{\frac{1}{2}} \tag{17}$$

In figure 22 the ratio of L_{f}/LG is plotted as a function of L/L_{g} (L_{g} is the frictionless tidal wave–length and $\mu = 0.6$). Now consider the length for which $L = L_{\mathrm{f}}$. It turns out that this length yields a good estimate of the maximum embayment length $L_{\max}$, as obtained with the full model (see figure 7).

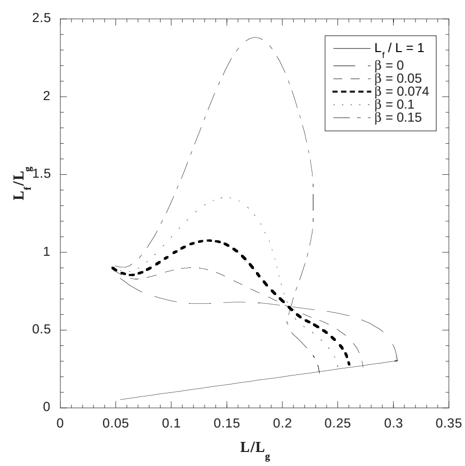

Figure 22: The dimensionless frictional length scale $L_{\mathrm{f}}/L_{\mathrm{g}}$ of the M_2 tide versus the dimensionless length of the embayment. Here L_{g} is the frictionless tidal wave-length and L_{f} has been computed using expression (17) with parameter $\mu = 0.6$. The water depths H_{f} and $H_{\max}$ are determined by the characteristics of the morphodynamic equilibrium. The intersection of these curves with the solid curve determines the maximum embayment length $L_{\max}$.

References

DE JONG, K. 1998. *Tidally averaged transport models*. Ph.D. thesis, Delft University of Technology.

DE SWART, H. E., & BLAAS, M. 1998. Morphological evolutions in a 1D model for a dissipative tidal embayment. *Pages 305–315 of:* DRONKERS, J.,

& SCHEFFERS, M. B. A. M. (eds), *Physics of Estuaries and Coastal Seas*. Rotterdam: Balkema, for PECS 1996.

DE VRIEND, H. J. 1996. Mathematical modelling of meso–tidal barrier island coasts. Part I: Empirical and Semi–Emperical Models. *Pages 115–149 of:* LIU, P.L.-F (ed), *Advances in coastal and ocean engineering*. World Scientific, Singapore.

DE VRIEND, H. J., & RIBBERINK, J. S. 1996. Mathematical modelling of meso–tidal barrier island coasts. Part II: Process–Based Simulation Models. *Pages 151–197 of:* LIU, P.L.-F (ed), *Advances in coastal and ocean engineering*. World Scientific, Singapore.

DYER, K. R., & SOULSBY, R. L. 1988. Sand transport on the continental shelf. *Ann. Rev. Fluid Mech.*, **20**, 295–324.

FOKKINK, R.J. 1998. *Morphodynamic network simulations of the Westerschelde*. report Z0919. Delft Hydraulics.

FRIEDRICHS, C. T. 1995. Stability shear stress and equilibrium cross–sectional geometry of sheltered tidal channels. *J. Coastal Res.*, **11**, 1062–1074.

FRIEDRICHS, C. T., & AUBREY, D. G. 1994. Tidal propagation in strongly convergent channels. *J. Geophys. Res.*, **99**, 3321–3336.

FRIEDRICHS, C.T., & MADSEN, O.S. 1992. Nonlinear diffusion of the tidal signal in frictionally–dominated embayments. *J. Geophys. Res.*, **97**, 5637–5650.

O'BRIEN, M. P. 1969. Equilibrium flow areas of inlets on sandy coasts. *J. Waterw. Harbors Div.*, **95**, 43–52.

POSTMA, H. 1954. Hydrography of the Dutch Wadden Sea. *Arch. Neerl. Zool.*, **10**, 405–511.

SCHIELEN, R., DOELMAN, A., & DE SWART, H. E. 1993. On the nonlinear dynamics of free bars in straight channels. *J. Fluid Mech.*, **252**, 325–356.

SCHUTTELAARS, H. M. 1997. *Evolution and stability analysis of bottom patterns in tidal embayments*. Ph.D. thesis, University of Utrecht, The Netherlands.

SCHUTTELAARS, H. M. 1999. *One–dimensional long–term equilibria of tidal embayments*. report R99–2. IMAU.

SCHUTTELAARS, H. M. to appear. Long–term modeling of channels and shoals in tidal embayments. PECS 1998.

SCHUTTELAARS, H. M., & DE SWART, H. E. 1996. An idealized long–term morphodynamic model of a tidal embayment. *Eur. J. Mech., B/Fluids*, **15**(1), 55–80.

SCHUTTELAARS, H. M., & DE SWART, H. E. 1999. Initial formation of channels and shoals in a short tidal embayment. *J. Fluid Mech.*, **386**, 15–42.

SCHUTTELAARS, H. M., & DE SWART, H. E. submitted. Multiple morphodynamic equilibria in tidal embayments. *J. Geo. Res.*

SEMINARA, G., & TUBINO, M. 1997. Bed formation in tidal channels: analogy with fluvial bars. *In:* DISILVIO (ed), *Morphology of rivers, estuaries and coasts*. IAHR Congress, London, contr. II.

THOOLEN, P. M. C., & WANG, Z. B. 1999. *Modelling of sediment transport in the Western Scheldt (in Dutch)*. report Z2489. Delft Hydraulics.

VAN DE KREEKE, J, & DUNSBERGEN, D. W. to appear. Tidal Asymmetry and Sediment Transport in the Frisian Inlet. PECS 98.

VAN DEN BERG, J.H., JEUKEN, C.J.L., & VAN DER SPEK, A.J.F. 1990. Hydraulic processes affecting the morphology and evolution of Westerschelde estuary. *Pages 157–184 of:* NORDSTROM, K.F., & ROMAN, C.T. (eds), *Estuarine shores: Evolution, Environments and Human Alterations*. Chichester: John Wiley and Sons Ltd.

VAN DER SPEK, A.J. 1997. Tidal asymmetry and long–term evolution of Holocene tidal basins in The Netherlands, simulation of paleo–tides in the Schelde estuary. *Marine Geology*, **141**, 71–90.

VAN RIJN, L. C. 1993. *Principles of sediment transport in rivers, estuaries and coastal seas*. Amsterdam: Aqua Publ.

VERBEEK, H., TANK, F.T.G., & GROENEWOUD, M.D. 1998. *Drempels in de Westerschelde, natuur en mens samen aan het werk*. Tech. rept. RIKZ.

WANG, Z.B., LOUTERS, T., & DE VRIEND, H.J. 1995. Morphodynamic modelling for a tidal inlet in the Wadden Sea. *Mar. Geol.*, **126**, 289–300.

ZIMMERMAN, J. T. F. 1992. On the Lorentz linearization of a nonlinearly damped tidal Helmholtz oscillator. *Proc. Kon. Ned. Akad. v. Wetensch.*, **95**, 127–145.